




RESEARCH ARTICLE | JUNE 05 2023

3D printing technique and its application in the fabrication of THz fibers and waveguides

Guofu Xu ; Maksim Skorobogatiy  *Journal of Applied Physics* 133, 210901 (2023)<https://doi.org/10.1063/5.0146054>View
OnlineExport
Citation

CrossMark

Articles You May Be Interested In

Characteristics of thermistors as temperature sensors on the sensor unit (SU-6803) and OP amp unit (OU-6801)

AIP Conference Proceedings (March 2021)

Arrangement for precision reciprocity calibration of condenser microphones

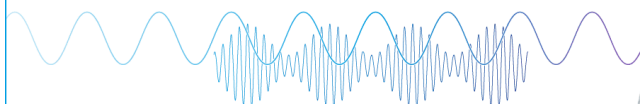
J Acoust Soc Am (November 1979)

A study of the valence photoelectron spectrum of uracil and mixed water–uracil clusters

J. Chem. Phys. (March 2023)

Webinar

Boost Your Signal-to-Noise Ratio with Lock-in Detection



Sep. 7th – Register now

Zurich
Instruments

3D printing technique and its application in the fabrication of THz fibers and waveguides

Cite as: J. Appl. Phys. 133, 210901 (2023); doi: 10.1063/5.0146054

Submitted: 9 February 2023 · Accepted: 9 May 2023 ·

Published Online: 5 June 2023



Guofu Xu and Maksim Skorobogatiy ^{a)}

AFFILIATIONS

Department of Engineering Physics, École Polytechnique de Montréal, Montréal H3T 1J4, Canada

^{a)}Author to whom correspondence should be addressed: maksim.skorobogatiy@polymtl.ca

ABSTRACT

3D printing, also known as additive manufacturing technique, has recently found applications in various engineering fields due to its ability to produce freeform 3D structures beyond the ability of traditional subtractive manufacturing methods. In this respect, the field of THz photonics is no exception. The adoption of 3D printing technique resulted in a revolution in THz optics and device manufacturing and will continue advancing this field for years to come. In this Perspective paper, we consider, in particular, the fabrication of guided optics devices for the THz operation range using additive manufacturing. We first introduce the technical characteristics of various 3D printing techniques as well as the advantages, disadvantages, and main performance parameters. Then, various 3D printed THz waveguides and fibers and functional devices, such as metalized/metallic/dielectric rectangular waveguides, photonic crystal waveguides, hollow-core anti-resonant/Bragg waveguides, hybrid metal/dielectric waveguides, plasmonic waveguide, porous fibers, magic tee, and serpentine waveguide traveling-wave circuits, are discussed. We also highlight practical applications of 3D printed waveguides/fibers in manipulating THz waves, especially in the fields of sensing and communication, including the analyte thickness and refractive index sensors, subwavelength/suspended core fiber communication links, dispersion compensators, and add-drop multiplexers. Finally, the prospects of 3D printing techniques in the THz field are summarized.

Published under an exclusive license by AIP Publishing. <https://doi.org/10.1063/5.0146054>

I. INTRODUCTION

The terahertz (THz) spectral range (0.1–10 THz) has seen a boom in many fields over the past two decades owing to advances in both generation and detection of THz waves, which has spurred countless technology companies to step into the spectrum, thus accelerating the practical applications of THz waves. Owing to the unique properties of THz waves, such as the non-ionizing nature,¹ large bandwidth,² strong absorption by water molecules,³ high directivity,⁴ etc., THz waves hold potential for a large spectrum of application in many fundamental and applied fields. It should be noted that some of these unique properties can pose disadvantages for specific applications. For example, high absorption by water molecules enables the THz wave application in label-free detection of abnormalities in biological tissues,⁵ while on the other hand, this property poses significant challenges for THz communications.^{6,7} Another example is the high directivity of THz waves, which gives the THz spectrum unique advantages in the field of secure communications,^{8,9} while, on the other hand, causing significant challenges in communication link

reliability by requiring high precision alignment between the transmitter and receiver antennas.¹⁰

THz waveguides and fibers, in particular, offer an effective way to manipulate THz radiation. A large variety of THz waveguides were developed for many applications including a suspended core fiber for label-free bacteria detection,¹¹ dielectric pipe waveguides for powder and liquid-vapor sensing,¹² dielectric/metamaterial/sapphire fibers for THz spectroscopy and imaging applications,^{13–15} various fiber/waveguide and fiber/waveguide-based functional devices for THz communication applications,¹⁶ and many others. With novel applications of THz waveguides and fibers, the techniques for THz waveguide/fiber fabrication have also evolved. The standard method of microstructured fiber fabrication is the drawing technique, which involves fabricating a structured preform, which is then pulled into the fiber under heating. There are several methods for THz fiber preform fabrication. The drilling technique is one of the most popular ones as the preform structure of virtually unlimited complexity can be milled using computer numerical control (CNC) machining.^{17–22} For example, the

23 August 2023 15:30:10

air-hole arrays with optimized structural parameters can be drilled in the solid plastic cylinder, with the resulting geometry transferred into the fiber during the drawing process. One of the disadvantages of the drilling technique, however, is the slow and laborious drilling process. Moreover, the drilled preforms are usually short and have a large diameter, which limits the length and quality of the drawn fibers. Alternatively, the stacking technique is commonly employed to fabricate fiber preforms of high porosity by bunching together (stacking) the thin wall tubes of circular or hexagonal shapes.^{23–26} Particularly, the preforms are fabricated by first assembling capillaries and rods in a desired pattern and then over-cladding the, thus, assembled stack with a larger tube to provide thermo-mechanical stability of the stack during the drawing process. One of the key disadvantages of this method is the heavy workload required by the stacking process as well as the geometrical limitation imposed by the process on the fiber structure. Another method used in microstructured fiber fabrication is preform casting technique,^{23,24,27,28} where polymer or glass is cast in a pre-made mold machined of metal, quartz, or other materials. This technique, while capable of producing consistently quality fibers from batch to batch, nevertheless, requires complex mold fabrication.

Note that all the above-mentioned techniques for preform fabrication still require a drawing step to get the actual fiber. Although the classic drawing technique developed for optical fiber fabrication can produce continuous kilometer-long strands, it is mostly suitable for the production of slender sub-mm filaments. In turn, THz fibers are typically much larger in diameter than optical fibers with outer diameters in a several mm-to-cm range. The limit of larger fiber diameters poses significant challenges for the drawing technique, which limits both the resultant fiber quality and their maximal length. In response to these challenges, the extrusion technique has been explored for the continuous fabrication of large-diameter fibers and preforms.^{29–32} Within this technique, the polymer billets or granules are melted and extruded through a die to fabricate fibers of a designed transverse structure. The key challenge for this technology is the laborious and expensive process of designing a complex and delicate die that has to be repeated every time a new fiber design is introduced.

Given the abovementioned limitations of the drawing and extrusion process for THz fiber fabrication, the advances in additive manufacturing techniques have opened new horizons for THz waveguides/fiber fabrication. Unlike traditional subtractive techniques (e.g., milling, cutting, etc.), the 3D printing technique, also known as the additive manufacturing technique, builds 3D structures layer-by-layer using the two-dimensional slices of a 3D model. 3D printing allows building complex freeform structures with a high degree of automation from a large variety of functional thermoplastic materials, which made this technique very popular with various applications such as medicine,^{33–35} aerospace,^{36–38} construction,^{39–41} clothing,^{42–44} and many others.^{45,46} In the field of electromagnetic waves, due to limited resolution (typically $\sim 200\text{ }\mu\text{m}$ for filament deposition modeling), the 3D printing technique was initially applied in relatively low-frequency ranges (such as radio frequencies).^{47–52} Most recently, further development of 3D printing techniques and the

improvement of printing resolution ($\sim 25\text{ }\mu\text{m}$ for stereolithography), has pushed the application of this technique to higher bands of the electromagnetic spectrum, such as THz waves. Furthermore, the most recent adaptation of classic 3D printing techniques allows printing infinitely long structures along a certain axis, thus opening a new avenue of research for the fabrication of THz fiber and fiber-based devices.

The paper is organized as follows. In Sec. II, we overview various 3D printing techniques that have been demonstrated for the fabrication of THz waveguide and fiber devices. In Sec. III, a brief overview of 3D-printed THz waveguides, fibers, devices, and circuits is presented. In Sec. IV, we highlight some most recent applications of the THz waveguide and fibers realized using 3D printing. Finally, in Sec. V, we conclude with a summary and discussion.

II. 3D PRINTING TECHNIQUES

To date, the 3D printing (additive manufacturing) technique has developed tremendously and can be classified into seven categories according to the process method,⁵³ which are directed energy deposition, sheet lamination, binder jetting, vat photopolymerization, material jetting, powder bed fusion, and material extrusion. Among them, direct energy deposition typically uses a high-power source (laser or electron beam) to extrude the melted material on the substrate layer-by-layer through a nozzle, during which an oxygen-free or vacuum environment is necessary. This technique is commonly used to repair worn or broken parts due to its relatively low resolution and poor surface finish. Sheet lamination, also known as laminated object manufacturing, fabricates 3D models by joining the precisely cut sheets/foils using adhesives or welding, which makes this technique features high fabrication efficiency and high surface finish but at the expense of availability of materials and layer heights. The binder jetting technique works by selectively jetting the adhesive binder to solidify the pre-sprayed powder, thus post-processing is required to cure the model and eliminate the binder material. Due to their respective limitations, the above three techniques are rarely applied to the fabrication of guided optics devices for the THz range. Thus, in the following of this perspective paper, we mainly focus on the last four 3D printing techniques that have been widely adopted for manufacturing THz-guided optics devices.

Vat photopolymerization is a technique based on selectively curing liquid photopolymer resin with a light source. Depending on the light source and curing procedure, this technique derives several sub-techniques, of which stereolithography (SLA) is the earliest developed and most widely used one.⁵⁴ For SLA technique, the resin is cured with ultraviolet (UV) light in a serial process (point-by-point), which results in a lengthy printing process. To improve the fabrication efficiency, a similar technique named digital light processing (DLP) was developed. This technique allows the resin to be cured layer-by-layer rather than point-by-point as a digital projector is used to flash cross-sectional images of the 3D model. Due to the same working principle, both of the above techniques have the advantages of high resolution, high dimensional accuracy, and smooth surface finish, while their applications are still limited due to

23 August 2023 15:30:10

disadvantages of high equipment investment, limited material availability, high cost of consumables, relatively small build volume, etc.

Material jetting has a working process similar to that of a two-dimensional inkjet printer. The material is dispensed selectively in the form of tiny droplets that are then cured by UV light. Depending on the material and system configuration, the material jetting technique spawns a variety of printing techniques, which are Polyjet printing (photosensitive resins), drop-on-demand printing (wax), and nanoparticle jetting (metal or ceramic particles). Among them, the Polyjet printing technique features relatively higher resolution, smoother surface finish, and higher fabrication efficiency as this technique allows for dispensing of multiple materials in a single print pass and the size of dispensed droplets is small. However, a supporting material (typically water-soluble polymer or wax) is required during printing, and thus, post-processing using sodium hydroxide solution or water jet to remove supporting structures is unavoidable after printing.

Powder bed fusion works on a similar principle to binder jetting, using material powder to build 3D models layer-by-layer. The difference is that powder bed fusion is a technique that uses a high-power source instead of a binder to selectively sinter the evenly distributed powder to form a solidified part. Depending on the adopted source, powder bed fusion has several different branch techniques, such as selective laser melting (SLM), selective laser sintering, and electron beam melting. As with direct energy deposition technique, an oxygen-free environment is required when using a laser source and a vacuum chamber is necessary while adopting an electron beam, which makes this technique one of the most expensive 3D printing techniques. Nevertheless, this technique has a high resolution and high surface finish due to the relatively small size of the metal powders ($\sim 10\text{--}100\mu\text{m}$).^{55–57} Among them, the SLM technique has a relatively high resolution that makes it possible to be applied for fabrication of guided optics at the THz range.

Material extrusion is one of the most cost-effective 3D printing techniques, with the most popular one being fused deposition modeling (FDM), also known as fused filament fabrication. This technique typically relies on vertically extruding melted thermoplastic onto a build platform through a heated nozzle. Due to such configuration, the resolution of FDM printers is limited by the size of extrusion heads that are generally in the scale of hundreds of micrometers. Nevertheless, owing to the cost-effective property and the wide availability of low-loss materials in the THz regime, the FDM 3D printing technique has been widely demonstrated for the fabrication of THz fibers. More importantly, a conveyor belt-based FDM printing technique, also known as infinity 3D printing technique, has recently been explored for the length-unlimited fabrication of microstructure THz fibers.⁵⁸ The emergence of infinity 3D printing technique is likely to break the volume limit of traditional FDM 3D printers and, thus, has the potential to become a powerful tool for long objects (e.g., fibers) fabrication and series production.

To simplify the comparison between the four 3D printing techniques focused on in this work, we summarize their key performance parameters along with the advantages and disadvantages in Table I.

TABLE I. Comparison of typical laboratory parameters of 3D printing techniques for THz waveguides fabrication.

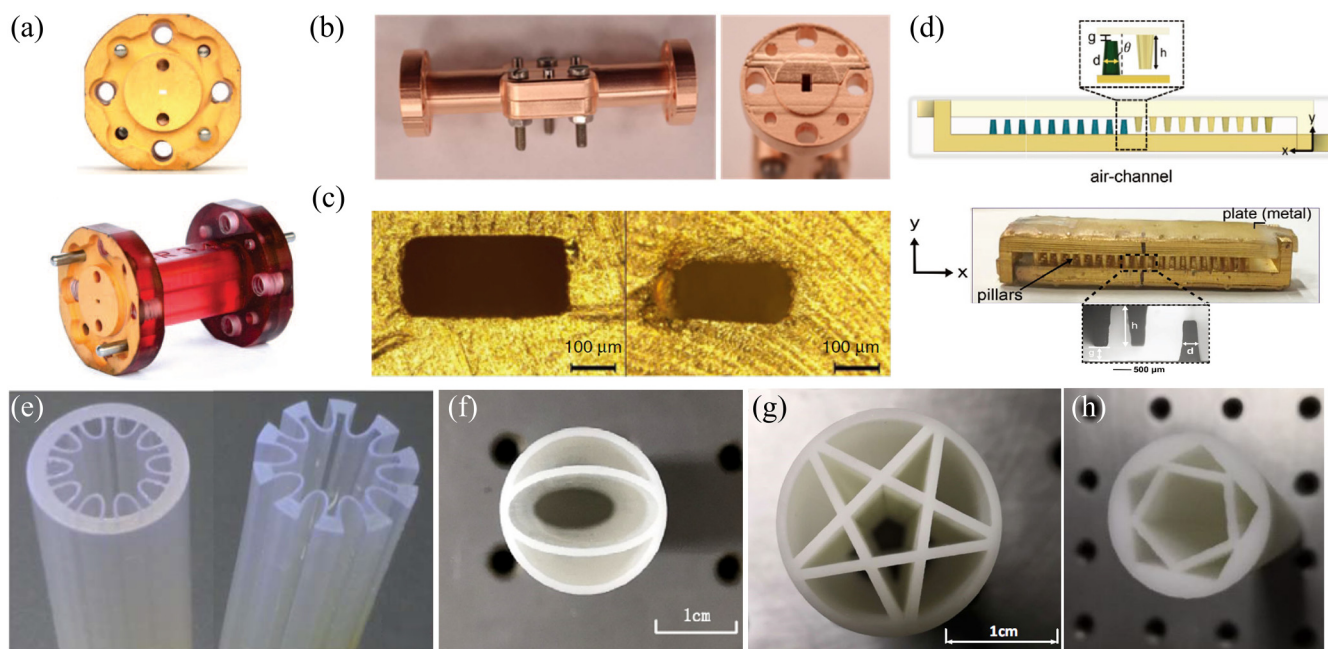
Type	Principle	Build volume (cm ³)	Layer height (μm)	Resolution (μm)	Material	Pros	Cons	Reference
SLA	Vat photopolymerization	$\sim (9\text{--}15) \times (5\text{--}15) \times (10\text{--}25)$	$\sim 10\text{--}300$	$\sim 25\text{--}150$	Photopolymer resin	High accuracy Smooth surface finish	Low efficiency Post-processing High cost	59–67 68–71
DLP		$\sim (4\text{--}10) \times (3\text{--}8) \times (20\text{--}25)$	$\sim 15\text{--}150$	$\sim 20\text{--}70$				
Polyjet	Material jetting	$\sim (25\text{--}35) \times (18\text{--}35) \times (15\text{--}20)$	$\sim 16\text{--}36$	$\sim 40\text{--}70$	Photopolymer resin	High efficiency High accuracy Smooth surface finish	Low mechanical strength Post-processing High cost	72–79
SLM	Powder bed fusion	$\sim (10\text{--}15) \times (10\text{--}15) \times (10\text{--}20)$	$\sim 20\text{--}100$	$\sim 40\text{--}100$	Metal	High accuracy High mechanical strength Smooth surface finish	High cost High cost Limited availability of materials	80 and 81
FDM	Material extrusion	$\sim (15\text{--}30) \times (15\text{--}30) \times (15 \times 30)$	$\sim 100\text{--}400$	$\sim 150\text{--}1000$	Thermoplastic	Cost-effective Wide availability of materials	Low-resolution Poor surface finish	58 and 82–88

III. 3D-PRINTED WAVEGUIDES/FIBERS

A. THz waveguides/fibers fabricated using vat photopolymerization

SLA or DLP, as one of the high-resolution 3D printing techniques, has been widely explored for the fabrication of THz waveguides/fibers. The early explorations using the SLA technique were aimed at realizing rectangular waveguides for applications in relatively low THz frequencies (below ~ 500 GHz). For instance, a 25 mm-long rectangular waveguide featuring a high aspect ratio was fabricated as a whole for the WR-3.4 band (220–330 GHz) using SLA technique [Fig. 1(a)].⁵⁹ Additional mechanical and chemical pretreatment steps were carried out after 3D printing the non-conducting photopolymer waveguides, and special attention was paid to optimize the plating process to achieve satisfactory copper layers on the waveguide surfaces. The transmission loss of the resultant waveguide in the WR-3.4 band was experimentally characterized to be ~ 12 – 16 dB/m, which is $\sim 50\%$ lower than that of a 1-in. long split-block aluminum alloy waveguide. This exploration shows that the SLA technique can be a competitive alternative

to traditional machining techniques for prototyping and production applications in the low THz range even though redundant pre- and post-processing procedures are necessary to achieve satisfactory performance. Another attempt was to fabricate a complete copper-plated WR-10 thru line [Fig. 1(b)] that is assembled with two individually printed split-block parts featuring a self-aligned design.⁶⁰ Before assembly, the two parts were metalized using electroless and electroplating techniques sequentially to achieve the desired metal (copper) layer thickness. The transmission loss of the fabricated WR-10 thru line was measured to be ~ 11 – 17 dB/m in the W-band. For the split-type manufacturing design, although the metallization process becomes easier to perform, the requirements for manufacturing precision are higher as additional losses can be introduced due to an imperfect assembly. In addition to the low THz range, the application of SLA technique in waveguide fabrication has also been extended to a higher THz range (above ~ 500 GHz). Recently, a novel SLA-based 3D printing technique, also known as “RECILS,” was developed, which enables high-precision thinning (~ 10 μm) printing.^{91,92} In conventional SLA techniques, the resolution is primarily influenced by the size of the UV light spot since



23 August 2023 15:30:10

FIG. 1. Various SLA printed waveguides: (a) Different views of the fabricated 25 mm-long rectangular waveguide featuring UG-387/UM flange for the WR-3.4 band.⁵⁹ Reproduced with permission from von Bieren *et al.*, in *2014 39th International Conference on Infrared, Millimeter, and Terahertz Waves (IRMMW-THz)* (IEEE, 2014). Copyright 2014 IEEE. (b) Different views of the fabricated 25 mm-long rectangular waveguide featuring UG-387/UM flange for the WR-3.4 band.⁶⁰ Reproduced with permission from D'Auria *et al.*, *IEEE Trans. Compon. Packag. Manuf. Technol.* **5**, 1339–1349 (2015). Copyright 2015 IEEE. (c) Cross-sectional micrographs of fabricated 5 mm-long metalized rectangular waveguides for WM-380 (left) and WM-250 (right) bands.⁶¹ Reproduced with permission from Otter *et al.*, *Electron. Lett.* **53**, 471–473 (2017). Copyright 2020 The Institution of Engineering and Technology. (d) Schematic and photo of the THz photonic crystal waveguide featuring the enclosure of pillars between parallel metallic plates. Inset: the microscope image of the air channel between two opposing pillars.⁶² Reproduced with permission from Khan *et al.*, *Adv. Mater. Technol.* **6**(7), 2100252 (2021). Copyright 2021 Wiley-VCH GmbH. (e) Negative curvature waveguide.⁶³ Reproduced with permission from Cruz *et al.*, in *2017 SBMO/IEEE MTT-S International Microwave and Optoelectronics Conference (IMOC)* (IEEE, 2017). Copyright 2017 IEEE; (f) elliptical waveguide.⁸⁹ Reproduced with permission from Yang *et al.*, *Opt. Fiber Technol.* **53**, 102064 (2019). Copyright 2019 Elsevier Inc.; (g) pentagram waveguide.⁹⁰ Reproduced with permission from Yang *et al.*, *J. Infrared Millimeter Terahertz Waves* **40**, 720–730 (2019). Copyright 2019 Springer Science Business Media; and (h) double pentagon nested hollow-core waveguide.⁹¹ Reproduced with permission from Yang *et al.*, *Opt. Fiber Technol.* **56**, 102199 (2020). Copyright 2020 Elsevier Inc.

each layer is solidified on the substrate submerged in a resin bath. In contrast, the RECILS technique enhances the resolution further by curing each layer in a precisely regulated narrow gap that contains ejected resin. Two 5 mm-long rectangular waveguides covering the 0.5–1.1 THz range were 3D printed using this technique and then metalized by electroless plating of 1 μm -thick nickel and 30 nm-thick gold as well as conventional plating of 1 μm -thick gold [Fig. 1(c)].⁶¹ The mid-band attenuations of the two waveguides were measured to be ~ 0.015 dB/m for the WM-380 band and ~ 0.04 dB/m for the WM-250 band, respectively. However, since this technique has only recently emerged and has not been widely adopted, its application in the fabrication of relatively large-size (a few centimeters) THz waveguides/devices remains to be validated.

In addition to metalized rectangular waveguides, the SLA technique has also been used to fabricate the THz topological photonic crystal waveguide where 2D hexagonally arranged photonic crystals composed of metallic pillars are oppositely attached to two confining parallel metallic plates [Fig. 1(d)]. Such a waveguide was realized by employing the split-type manufacturing design and gold sputtering technique. The fabricated waveguides were demonstrated to have a transmission loss of less than ~ 0.4 dB/m in the bandgap of

~ 147 – 157 THz as well as the capability of robust light guidance immune to structural defects and sharp bends. The limitations of the proposed waveguide are the high coupling loss (~ 10 dB) and the high precision requirement in pillar fabrication. Moreover, the size of such a waveguide has to be large enough to allow more pillars to be accommodated as cladding to grant the waveguide sufficient wave confinement ability. Another type of waveguide that has been implemented with the SLA technique is the hollow-core waveguide as the THz wave can be guided in the lossless air cavity rather than the lossy photopolymer resin. Figures 1(e) and 1(f) show the SLA-printed hollow-core waveguides featuring diameters and lengths in the range of ~ 1 – 2 cm and ~ 10 – 15 cm and losses of ~ 5 – 80 dB/m in the 0.4– 2 THz band. An obvious limitation of these waveguides is their flexibility due to the high loss of the photopolymer resin that necessitates the use of large air cores to reduce the interaction between the core-guided mode and cladding.

Similar to SLA technique, the early explorations of the DLP technique were also for realizing metalized rectangular waveguides. Two conventional rectangular waveguides for W and D bands were obtained using the DLP technique in combination with electroless silver and copper plating [Fig. 2(a)].⁶⁸ The insertion loss of the

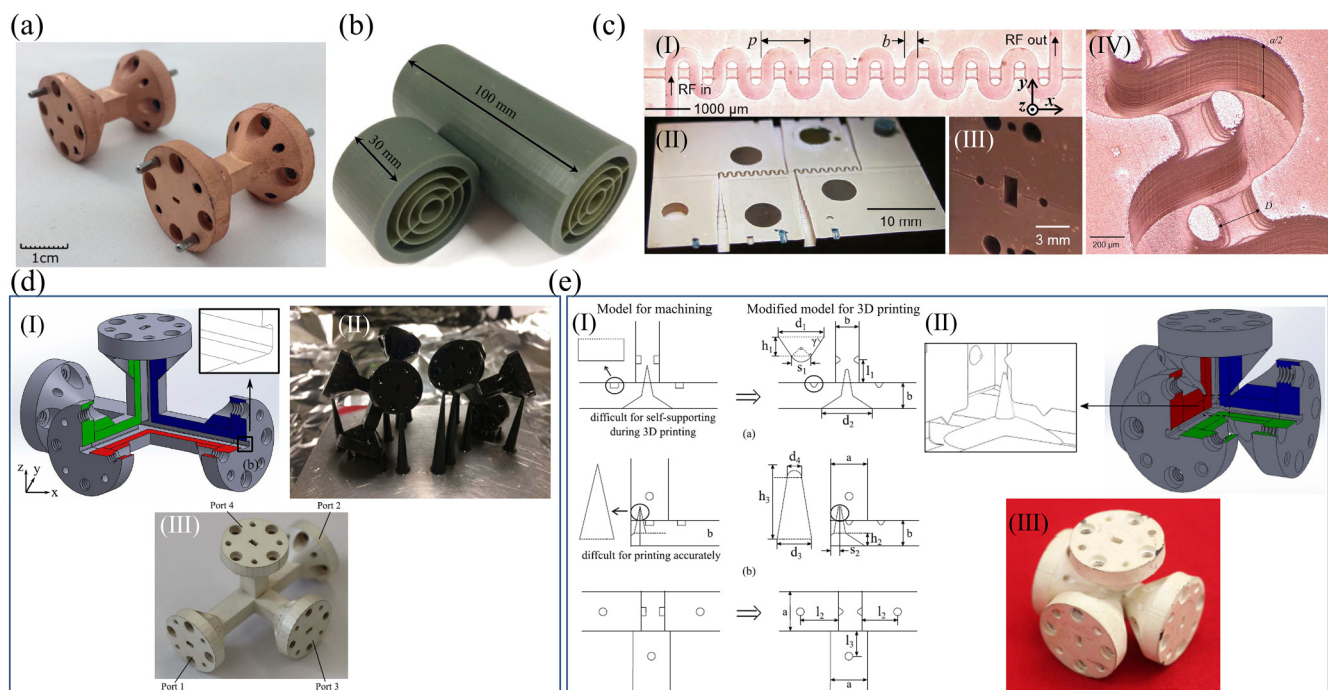


FIG. 2. Various DLP printed waveguides: (a) Photo of the 25.4 mm-long metalized rectangular waveguide for W (left) and D (right) bands.⁶⁸ Reproduced with permission from Shen *et al.*, in 2017 IEEE MTT-S International Microwave Symposium (IMS) (IEEE, 2017). Copyright 2017 IEEE. (b) The photographs of the fabricated THz Bragg fibers.⁶⁹ Reproduced with permission from Hong *et al.*, IEEE Trans. Terahertz Sci. Technol. **8**, 90–99 (2018). Copyright 2018 IEEE. (c) The fabricated serpentine waveguide traveling-wave circuit for the W band. (I) Top view of the half split-block circuit. (II) Half split block containing two circuits, integrated waveguide transitions, and alignment holes. (III) WR-10 waveguide opening of the assembled split blocks. (IV) Enlarged view of the serpentine waveguide.⁷⁰ Reproduced with permission from Cook *et al.*, IEEE Access **7**, 72561–72566 (2019). Copyright 2019 IEEE. (d) Traditional W-band magic tee: (I) The 3D model with the curved corner design optimized for DLP 3D printing. (II) Samples printed at a 45° angle to the build platform. (III) Metalized samples. (e) Broadband W-band magic tee: (I) Optimization on conventional structures with round-tip structures for self-supporting in the DLP 3D printing process. (II) Cross-sectional view of the proposed model and the enlarged view of the central complex structure. (III) Metalized samples.⁷¹ Reproduced with permission from Shen and Ricketts, IEEE Trans. Microw. Theory Tech. **67**, 883–895 (2019). Copyright 2019 IEEE.

W-band waveguide and the transducer loss of the D-band waveguide were measured to be ~ 4.7 – 9.8 and ~ 10.2 – 39.8 dB/m, respectively. In addition, in Ref. 69, an all-dielectric (EnvisionTEC HTM 140) hollow-core Bragg fiber featuring a diameter of ~ 2.3 cm was fabricated up to 10 cm using the DLP technique [Fig. 2(b)]. The propagation loss was measured to be ~ 3 – 5 dB/m in the single-mode operation frequency range of 246–276 GHz. In recent years, some attempts of using 3D printing techniques to fabricate waveguides with complex geometries have been carried out. Figure 2(c) shows an example of such a waveguide that features a serpentine traveling-wave tube.⁷⁰ The waveguide was implemented in a split-block configuration and contains multiple complex structures (serpentine circuits, integrated waveguide transitions, etc.) and assembly features. After gold sputtering and copper electroplating, two completed waveguide circuits (W and D bands) were demonstrated to have insertion losses of ~ 0.55 dB at 95 GHz and ~ 2.4 dB at 140 GHz, respectively. Though the performance of the 3D printed traveling-wave tube circuits is comparable to that of ideal smooth-wall circuit simulations, the devices achievable by this technique are still limited to low-power upper-millimeter wave passive components or low average power active vacuum electron devices due to limitations (low thermal conductivity, low melting point, etc.) imposed by plastic materials. Another example of using DLP printing is the implementation of traditional and broadband magic tee for W-band applications.⁷¹ These devices were DLP printed in combination with a curved corner design [panel I of Fig. 2(d)] and an off-axis print angle [panel II of Fig. 2(d)]. Moreover, the broadband magic tee adopts round-tipped structures rather than sharp-tipped structures of traditional magic tees [panels I and II of Fig. 2(e)], which eases the fabrication using 3D printing. The insertion losses of the two magic tees were measured to be less than ~ 1.3 and ~ 5.5 dB in the W-band, which are no better than performances of CNC-machined magic tees. Thus, for such a complex device, a well-designed structure and finely optimized printing process are required to achieve satisfactory quality. Moreover, a complex metallization process, including wetting, seeding, plating, and passivating, is indispensable to achieve robust performance. Furthermore, the mechanical strength of the printed devices remains to be verified, which also brings challenges for its practical application. In addition, a recent exploration of manufacturing complex THz waveguide components⁹⁴ reveals that the printing orientation has a certain impact on the surface profile and dimensional accuracy, which deserves special attention for high quality manufacturing.

B. THz waveguides/fibers fabricated using material jetting

Material jetting has also been widely used in various waveguide fabrication applications due to its relatively high resolution despite being less mechanically robust than vat photopolymerization. The most common waveguides fabricated with this technique are hollow-core waveguides. Figure 3(a) shows an all-dielectric hollow-core photonic crystal waveguide (~ 37 mm in diameter) fabricated using this technique.^{72,95} During fabrication, water-soluble supporting material is required to provide a substrate upon which the waveguide material can be printed. The fabricated waveguides

(up to 15 cm long) were demonstrated to have several low-loss transmission gaps in the 80–240 GHz range, with the lowest loss of ~ 30 dB/m at ~ 105 GHz. Subsequently, a photonic crystal antenna (8.5 cm in length and 16 mm in diameter) [Fig. 3(b)] that is extremely difficult to be realized with the drawing or extrusion technique was fabricated in the same way based on the above waveguide design.⁷³ Four highly directional passbands at ~ 105 , 120, 150, and 170 GHz were clearly observed, which present comparable radiation performance to a copper horn antenna with the same geometry. Another waveguide of the same type is shown in Fig. 3(c), which was fabricated up to 30 cm long (~ 26 mm in diameter) by mechanically splicing two short waveguide segments.⁷⁴ The averaged power loss of the fabricated waveguide was characterized to be ~ 8.7 dB/m over 0.2–1 THz range, with the minimum value of ~ 0.9 dB/m achieved at 0.75 THz. The main limitation of such photonic crystal waveguides is poor flexibility and relatively narrow bandwidth, which limits the variety of practical applications.

To realize the broadband low-loss transmission of THz waves, two different types of hollow-core waveguides have also been implemented using the material jetting technique, which are metal wire embedded hybrid⁷⁵ and anti-resonant surface clad⁷⁶ hollow-core waveguides. The wire-embedded waveguides [Fig. 3(d)] were fabricated by manually inserting copper wires into the selected holes of 3D printed polymer waveguides (up to 10 cm long), which ignores the thermal incompatibility of two different materials that needs to be considered in drawing similar fibers. The anti-resonant hollow-core waveguide [Fig. 3(e)] was directly 3D printed (up to 10 cm) using a Polyjet printer; however, the designed sharp-tipped cones that are difficult to achieve in 3D printing were printed imperfectly into round-tipped cones [see panel III in Fig. 3(e)]. The broadband transmission (up to 1 THz) of THz waves was experimentally observed for the fabricated waveguides. However, the fabricated waveguides were demonstrated to be relatively lossy (tens of dB/m) due to the small hollow core (~ 3 – 4 mm); thus, a large air core is necessary for such waveguides to support low-loss guidance of THz waves, but meanwhile, one has to be cautious about the suppression of higher order modes in large core waveguides. Although THz broadband transmission has also been demonstrated with dielectric ridge waveguides (up to 3 cm long) [Fig. 3(f)], this type of waveguide proved to be quite lossy (large than $\sim 10^2$ dB/m) due to the high material loss of the photosensitive polymer.⁷⁷ In addition to the above, by combining with metallization techniques, the material jetting technique has also been used to realize plasmonic waveguides/devices (up to 10 cm) [Fig. 3(g)], including straight planar waveguides, non-planar waveguides, and splitters.⁷⁸ These waveguides/devices were made by sputtering a gold layer on 3D-printed waveguide substrates. Due to such a fabrication process, the manufactured devices are relatively lossy (~ 74 dB/m at ~ 270 GHz), which is mainly attributed to the rough substrate surface and the unevenness of the gold layer. Therefore, a delicate metallization process as well as the pre-optimization and post-processing procedures that can improve the surface roughness, are key guarantees for the good performance of such metallized 3D printed waveguides/devices. Ultimately, strong mechanical strength is the last propellant for the practical application of these waveguides, which is unfortunately one of the drawbacks of the material jetting technique.

23 August 2023 15:30:10

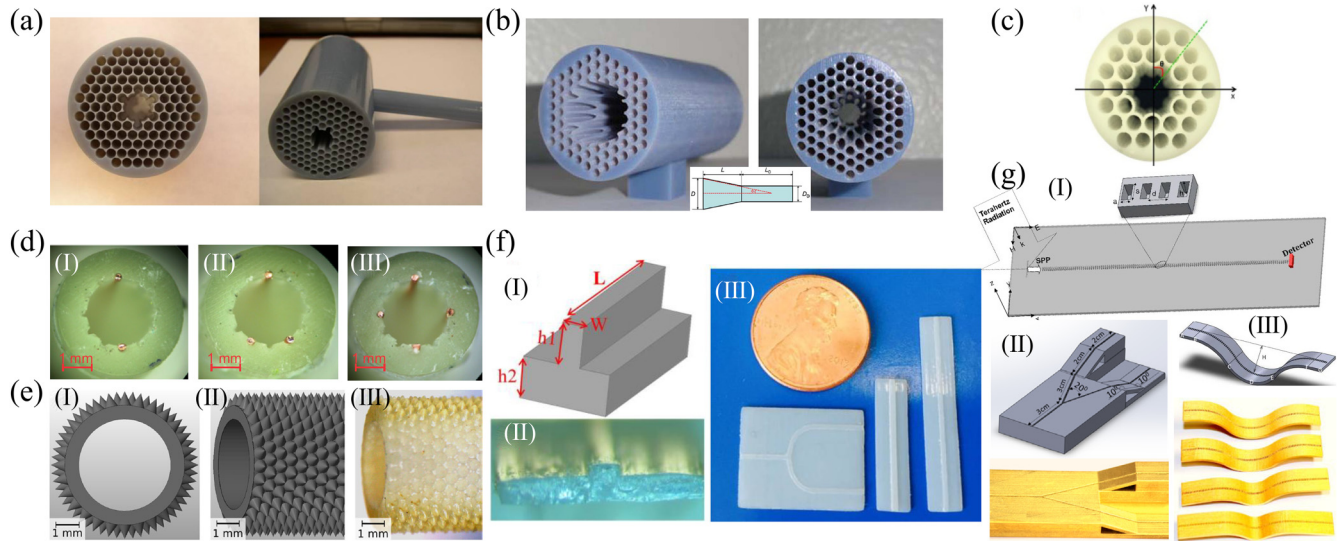


FIG. 3. Various waveguides fabricated with material jetting technique: (a) Hollow-core photonic crystal waveguide.⁷² Reproduced with permission from Wu *et al.*, *Opt. Express* **19**, 3962–3972 (2011). Copyright 2011 Optical Society of America. (b) Hollow-core photonic crystal waveguide-based horn antenna. Inset: side view schematic of the antenna.⁷³ Reproduced with permission from Wu *et al.*, *IEEE Trans. Antennas Propag.* **60**, 5557–5563 (2012). Copyright 2012 IEEE. (c) Cross-sectional view of the photonic crystal waveguide.⁷⁴ Reproduced with permission from Yang *et al.*, *Opt. Express* **24**, 22454–22460 (2016). Copyright 2016 Optical Society of America. (d) Hollow-core waveguides with (I) two-wire, (II) three-wire, and (III) four-wire configurations.⁷⁵ Reproduced with permission from Yudasari *et al.*, *Opt. Express* **22**, 26042–26054 (2014). Copyright 2014 Optical Society of America. (e) Hollow-core anti-resonant waveguide: (I) cross section and (II) side view of the waveguide 3D model. (III) Side view of the fabricated waveguide.⁷⁶ Reproduced with permission from Vogt and Leonhardt, *J. Infrared Millimeter Terahertz Waves* **37**, 1086–1095 (2016). Copyright 2016 Springer Science Business Media New York. (f) The fabricated ridge waveguides and splitter: (I) 3D schematic, (II) side view, and (III) photo.⁷⁷ Reproduced with permission from Kaur *et al.*, in *2015 IEEE 65th Electronic Components and Technology Conference (ECTC)* (IEEE, 2015). Copyright 2015 IEEE. (g) 3D schematics and photos of the (I) straight waveguide, (II) Y-splitter, and (III) curved waveguides.⁷⁸ Reproduced with permission from Pandey *et al.*, *Opt. Express* **21**, 24422–24430 (2013). Copyright 2013 Optical Society of America.

C. THz waveguides/fibers fabricated using powder bed fusion

As a sub-category of powder bed fusion, SLM technique is the one that can provide the highest mechanical strength. This technique typically builds models by selectively melting metal powders using a high-energy laser in an oxygen-free environment. Although for economic reasons, the SLM technique is not as popular in the

field of laboratory research as the other 3D techniques highlighted in this paper, it has also been used in small quantities in the fabrication of THz horn antennas,^{96,97} waveguide transitions,⁹⁸ reflective optics,⁸¹ and metal waveguides.^{80,99,100} The first SLM printed rectangular waveguide (Ti-6Al-4V alloy) was demonstrated to have an insertion loss of ~ 1.5 dB at 94 GHz after the surface is smoothed with abrasive blasting and chemical polishing [Fig. 4(a)].⁸⁰

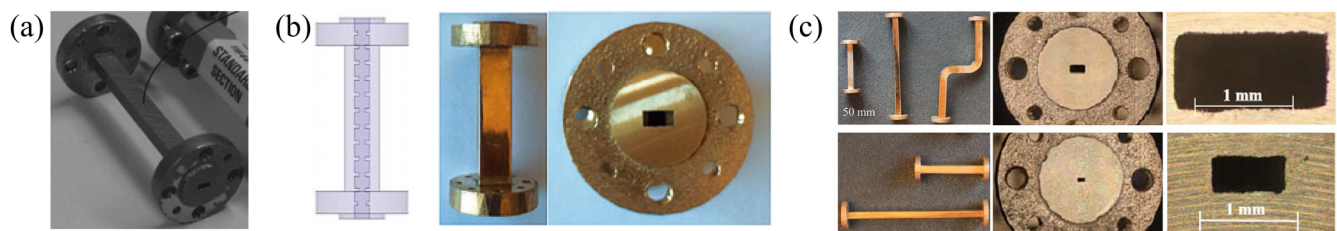


FIG. 4. Various SLM printed waveguides: (a) Photo of the 50 mm-long WR-10 rectangular waveguide.⁸⁰ Reproduced with permission from Caekenberghe *et al.*, *Microw. Opt. Technol. Lett.* **54**, 2572–2575 (2012). Copyright 2012 Wiley Periodicals Inc. (b) Schematic, photo, and cross-sectional view of the standard WR-12 rectangular waveguide-based bandpass filter.⁹⁹ Reproduced with permission from Zhang and Zirath, *Electron. Lett.* **51**, 1791–1793 (2015). Copyright 2020 The Institution of Engineering and Technology. (c) Photos and cross-sectional views of the 50 mm-long or 100 mm-long straight and curved rectangular waveguides for D (top) and H (bottom) bands.¹⁰⁰ Reproduced with permission from Zhang and Zirath, *IEEE Trans. Compon. Packag. Manuf. Technol.* **6**, 796–804 (2016). Copyright 2016 IEEE.

Subsequently, a rectangular waveguide-based bandpass filter was implemented by SLM using CuSn_{15} alloy powder.⁹⁹ The measured passband of the fabricated device [Fig. 4(b)] is $\sim 84\text{--}90$ GHz with an average passband insertion loss of ~ 3 dB and stopband attenuation of ~ 50 dB. Hereafter, the application of SLM technique in waveguide fabrication was pushed to higher frequencies. Several 50 or 100 mm-long straight and curved waveguides were printed with CuSn_{15} alloy powder for applications in D (110–170 GHz) and H (220–325 GHz) bands.¹⁰⁰ The average dissipative attenuation and bending loss of the D-band waveguides [top panel in Fig. 4(c)] were measured to be ~ 20 dB/m and ~ 1.79 dB per 90° bend, which are $\sim 2\text{--}3$ times higher than that of the commercial D-band waveguides. The average dissipative attenuations of the SLM printed H-band waveguides [bottom panel in Fig. 4(c)] are ~ 94 dB/m (50 mm-long) and ~ 120 dB/m (100 mm-long), which are $\sim 1.1\text{--}1.5$ times higher than that of commercial H-band waveguides. In conclusion, manufacturing metallic rectangular waveguides with SLM technique offers process simplicity and can provide good mechanical robustness. For relatively low THz frequencies (~ 0.1 THz), such additive manufacturing process enables fabricated devices with comparable performance to commercial waveguides. To improve the performance of SLM-printed metallic waveguides at higher THz frequencies, more precise dimensional control and smoother surface finish are required, which will surely be improved with future advances in SLM printers and applicable materials. Of course, further improvement in device performance through physical (e.g., sandblasting and micromachining) and chemical polishing

processes has also proven to be an effective approach; nevertheless, delicate attention needs to be devoted.

D. THz waveguides/fibers fabricated using material extrusion

Material extrusion or FDM-based 3D printing technique, as the most cost-effective additive manufacturing technique, has been widely used in the laboratory research for the fabrication of various THz optics, such as prisms,^{101,102} lenses and gratings,^{103–109} reflectors,¹¹⁰ etc. In terms of THz fiber fabrication, this technique is typically utilized in two ways. One is to extrude microstructured preforms or fibers through a pre-designed die, several examples of which are shown in Figs. 5(a)–5(c). Similar to fiber drawing technique, the die extrusion technique has the advantage of high production efficiency. However, it has a complex die design process and also requires precise calibration and monitoring during the drawing process to obtain the final satisfactory fiber dimension and quality. Therefore, it is quite difficult to obtain long fibers with consistent quality in this way. The typical lengths of these fibers that have been extruded are below ~ 8 cm, and the experimentally measured losses are about tens to hundreds of dB/m in $\sim 0.4\text{--}1$ THz frequency range.^{30–32} The other one is the traditional FDM 3D printer that fabricates microstructured fibers by depositing vertically layer-by-layer on the build platform through a circular orifice nozzle (usually above $\sim 200\ \mu\text{m}$ in diameter). Due to the limited resolution, this technique is often used to realize large-

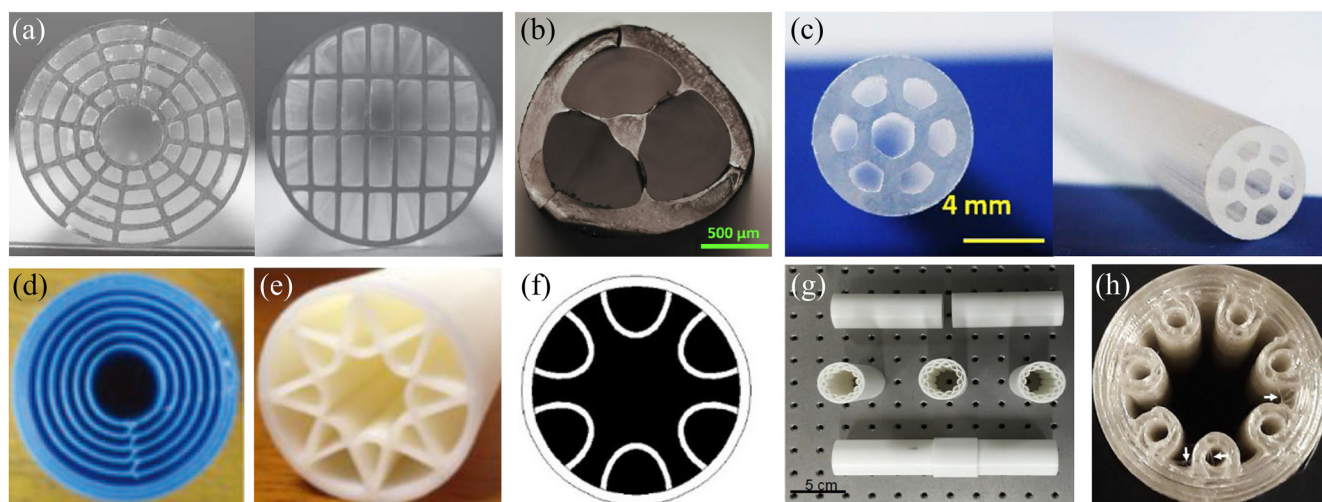


FIG. 5. Various FDM extruded or printed preforms and fibers: (a) Cross-sectional view of the extruded spider-web (12 mm diameter) and rectangular (10 mm diameter) porous preforms.³⁰ Reproduced with permission from Atakaramians *et al.*, *Opt. Express* **17**, 14053–14062 (2009). Copyright 2009 Optical Society of America. (b) Cross-sectional view of the extruded suspended core fibers.³¹ From Talataisong *et al.*, *Sci. Rep.* **10**, 11045 (2020). Copyright 2020 Author(s), licensed under the Creative Commons Attribution 4.0 International License. (c) Photos of the extruded hollow-core anti-resonant fiber.³² From Talataisong *et al.*, *Photon. Res.* **9**, 1513(2021). Copyright 2021 Author(s), licensed under the Creative Commons Attribution 4.0 International License. (d) Cross-sectional view of the printed Bragg fiber.⁶² Reproduced with permission from Cruz *et al.*, in *2015 40th International Conference on Infrared, Millimeter, and Terahertz Waves (IRMMW-THz)* (2015). Copyright 2015 IEEE. (e)–(h) Photo or schematic of printed hollow-core anti-resonant fibers.^{83–86} (e) Reproduced with permission from Cruz *et al.*, *J. Microw. Optoelectron. Electromag. Appl.* **14**, 45–53 (2015). Copyright 2015 JMOe. (f) From van Putten *et al.*, *Appl. Opt.* **57**, 3953–3958 (2018). Copyright 2018 Author(s), licensed under the Creative Commons Attribution 4.0 International License. (g) Reproduced with permission from Li *et al.*, *Optik* **176**, 611–616 (2019). Copyright 2018 Elsevier GmbH. (h) Reproduced with permission from Sultana *et al.*, *IEEE Trans. Terahertz Sci. Technol.* **11**, 245–260 (2021). Copyright 2021 IEEE.

23 August 2023 15:30:10

diameter fibers such as hollow-core Bragg fibers or hollow-core anti-resonant fibers [Figs. 5(d)–5(h)]^{82–86} that feature diameters and lengths in the range of ~ 1 –4 cm and ~ 2 –15 cm, respectively. The typical transmission losses of those fibers are characterized to be tens to hundreds of dB/m in ~ 0.1 –1 THz. Due to their large size and easily accessible mode fields enclosed in the hollow core, these fibers are generally suitable for sensing applications.

IV. 3D PRINTED WAVEGUIDES/FIBERS FOR THz SENSING AND COMMUNICATION APPLICATIONS

In this section, we highlight some recently realized 3D printed THz waveguides/fibers and functional devices for practical applications, including several Bragg waveguides realized by various 3D printing techniques (SLA, FDM, Polyjet) for sensing applications, rod-in-air and suspended core fibers realized via FDM printing technique for THz communications, as well as two functional communication devices (dispersion compensators and add-drop multiplexer) realized using SLA 3D printing and chemical metallization techniques. It is worth emphasizing that 3D printing techniques have been extensively applied in many fields within the THz regime (e.g., THz imaging, etc.),^{111–118} while this section is not intended to cover all the applications of 3D printed THz optics but rather to highlight several applications of 3D printed fibers/waveguides and functional devices.

Among the various 3D printing technologies mentioned above, although some of them (e.g., vat photopolymerization and material jetting) have relatively high resolutions, the high absorption loss of printing materials (e.g., photosensitive resin, polylactic acid, acrylonitrile butadiene styrene) limits the application of 3D printing techniques in the fabrication of direct light-guiding structures (fiber core). Therefore, avoiding this shortcoming by appropriate fiber design is a way to promote its practical applications. Hollow-core Bragg waveguide typically consists of a low-loss gas-filled hollow core and multiple alternating concentric layers with two different refractive indices is such an example. Such configuration could result in the forbidden propagation of a specific electromagnetic frequency band, which is referred to as a photonic bandgap. The loss-loss and low-dispersion guidance can be achieved with Bragg waveguides that feature a low-loss gas-filled hollow core as the light within the bandgap will be confined and propagate in the low-loss air cavity. The center frequency and width of the bandgap can be finely tuned simply by adjusting the thickness and refractive index of these layers. The periodic refractive index variation of the reflective layers of a Bragg fiber can be achieved in various ways, such as alternately repeating polymers with different refractive indices^{119–123} and periodically introducing air or porous rings.^{18,30,124,125} Another type of Bragg fibers is realized by employing periodic lattice cladding,^{126,127} which could achieve bandgap with low loss via high porosity. In the following, we will introduce two hollow-core Bragg fibers realized using SLA/FDM techniques and their applications in the field of THz sensing as well as a hyperuniform disordered Bragg fiber implemented with Polyjet 3D printing.

To date, many THz fiber-based sensors have been proposed thanks to extended detection depths achievable with THz waves, such as amplitude modality-based suspended-core waveguide

sensors¹¹ and anti-resonant THz waveguide sensors that utilize the spectral shift of the resonant wavelength.^{12,128–130} The detection sensitivities of most of the above-mentioned sensors are limited due to their relatively broad transmission spectrum. It has been demonstrated that such limitations can be mitigated by using sensors with narrow resonances.^{131,132} Figure 6(a) presents such an example realized using the SLA printing technique. The improvement in the detection limit of the Bragg waveguide sensor was achieved by introducing a geometrical defect in the first layer of the Bragg reflector, which results in a narrow spectral loss peak into the broad transmission band.⁶⁴ Such effectively single-mode (HE₁₁-like) broadband (~ 50 GHz) Bragg waveguide [see Fig. 6(b)] was optimized to have a 4.5 mm (diameter) circular hollow core surrounded by 10 periodic high (photosensitive resin) and low (air) refractive index bilayers with a thickness of $512\ \mu\text{m}$. By introducing a defect layer [blue layer in Fig. 6(a)] on the inner surface of the hollow core, anti-crossing between the core-guided HE₁₁ mode and localized defect mode occurs [Fig. 6(c)], leading to a significant increase in the waveguide propagation loss [see Inset in Fig. 6(c)]. Thus, the sensing functionality can be achieved by tracking the offset of the anti-crossing frequency as this frequency is strongly dependent on the defect layer thickness. As shown in Fig. 6(d), by comparing the transmission spectra of the 2.5 cm-long modified Bragg waveguide (optimized defect layer thickness of $300\ \mu\text{m}$) inserted with different thicknesses (0, 50, and $100\ \mu\text{m}$) of PMMA films [Fig. 6(d)], one can observe a linear dependence between the resonant dip and the film thickness. As a result, a surface sensitivity of $0.1\ \text{GHz}/\mu\text{m}$ was experimentally achieved.

It is important to note that the shift in the anti-crossing frequency depends not only on the thickness but also on the refractive index of the target analyte. The above case considers target analytes of different thicknesses with a fixed refractive index, while the next case considers target analytes of different refractive indices with a fixed thickness. More importantly, both amplitude and phase modalities were employed in the latter case.⁸⁷ Figure 6(e) presents the band diagram of the resonant fluidic sensors realized with an FDM-printed Bragg waveguide. The waveguide was designed to have a rectangular hollow core (4.5 mm side length) and 10 periodic high (Polylactic Acid) and low (air) refractive index bilayers (1.6 mm thickness). By introducing a defect layer (fluidic) in the reflector second layer (air) [see inset in Figs. 6(e) and 6(f)], the loss peak (transmission dip) can be induced owing to the anti-crossing phenomenon. As shown in Fig. 6(g), by tracking the frequency shift of the transmission dip, changes in the refractive index of an analyte featuring fixed thickness can be monitored. A sensitivity of $\sim 113.7\ \text{GHz}/\text{RIU}$ and a resolution of $\sim 8.0 \times 10^{-3}\ \text{RIU}$ were experimentally achieved within the amplitude detection modality. The phase detection modality of the sensor can be realized based on the principle that a sudden change is involved in the dominant mode effective refractive index when going through the anti-crossing region. Such sudden effective refractive index variation will lead to a step-like shape in the sensor phase response [Fig. 6(h)]. As a result, a comparable sensitivity of $\sim 111.1\ \text{GHz}/\text{RIU}$ was obtained within the phase detection modality, while higher resolution ($\sim 4.5 \times 10^{-3}\ \text{RIU}$) can be achieved compared to the amplitude modality owing to the mitigated effects of the standing wave when working with a normalized signal phase.

23 August 2023 15:30:10

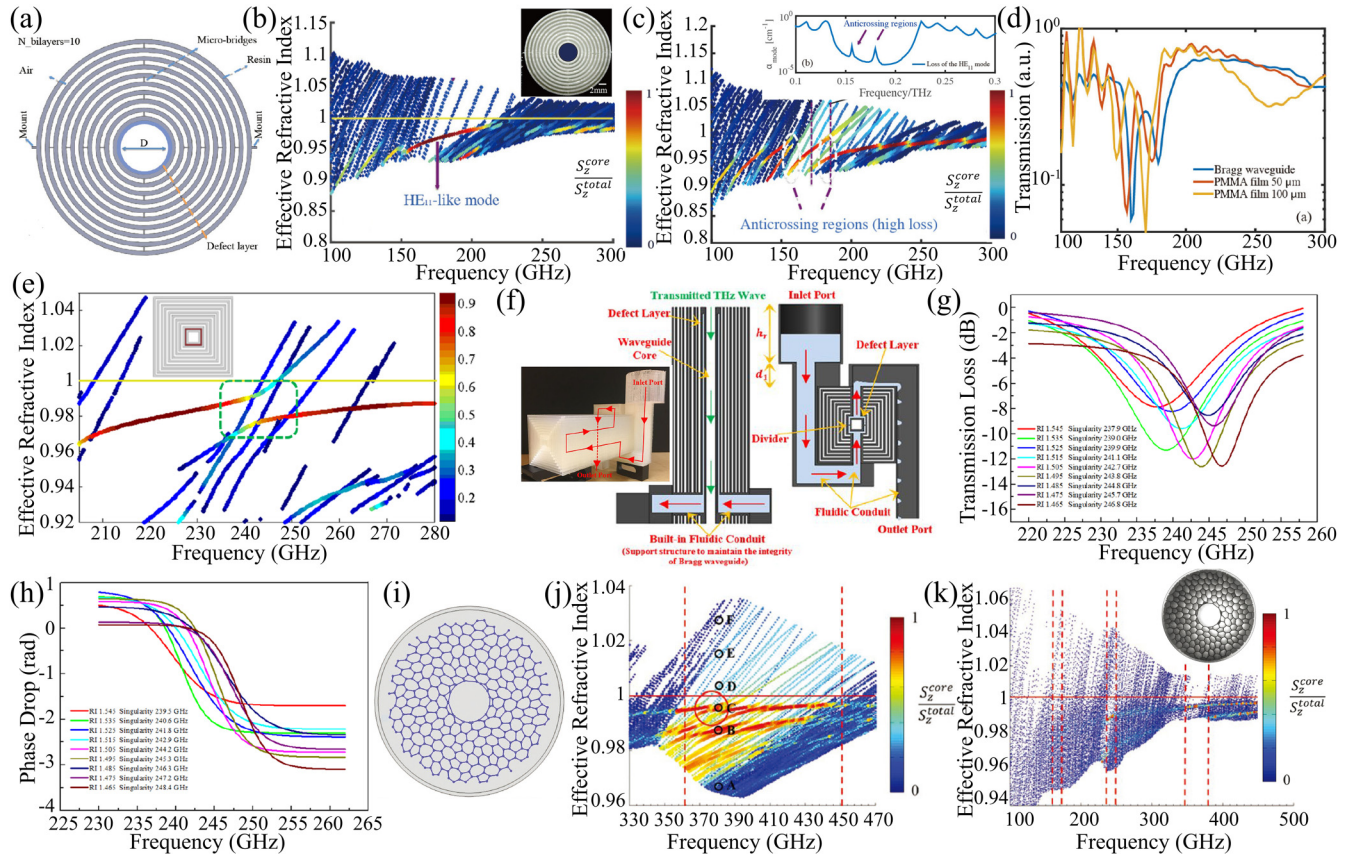


FIG. 6. (a) Schematic of the Bragg waveguide cross section. The gray, white, and light blue regions represent photosensitive resin, air, and the defect in the first reflector layer. (b) Band diagram of the Bragg waveguide without the defect layer. Inset: photo of the SLA-printed Bragg waveguide cross section. (c) Band diagram of the Bragg waveguide with a 300 μm -thick defect layer. Inset: Propagation loss of the fundamental mode in the anti-crossing region. (d) Measured transmission spectra of the Bragg waveguide (with a 300 μm -thick defect layer) with PMMA films of different thicknesses (0, 50, and 100 μm) inserted into the waveguide core.⁶⁴ Reproduced with permission from Li *et al.*, *Opt. Express* **25**, 4126–4144 (2017). Copyright 2017 Optical Society of America. (e) Band diagram of the Bragg waveguide with a defect in the second reflector layer. Inset: schematic of the cross section of a Bragg waveguide with a defect layer. (f) The photo and schematic of the FDM printed 10 cm-long THz Bragg waveguide-based fluidic sensor. The gray, blue, and white regions represent the polymer material, liquid analyte, and air. The red and green arrows show the directions of the flowing liquid analyte and THz propagation. Normalized and fitted experimental (g) transmission and (h) phase dependence curves in the vicinity of the absorption peak for different refractive indices of analytes.⁶⁷ Reproduced with permission from Cao *et al.*, *Opt. Express* **27**, 27663–27681 (2019). Copyright 2019 Optical Society of America. (i) The cross-sectional view and (j) band diagram of the designed Bragg waveguide featuring hyperuniform disordered reflectors. (k) The band diagram of the 3D printed (Polyjet) waveguide with bridge thicknesses of 200 μm . Inset: Cross section of the fabricated waveguide.⁷⁹ Reproduced with permission from Ma *et al.*, *Adv. Opt. Mater.* **4**, 2085–2094 (2016). Copyright 2016 Wiley-VCH Verlag GmbH & Co. KGaA, Weinheim.

In addition to the above SLA/FDM printed Bragg waveguide with purely periodic structures, a novel Bragg waveguide utilizing hyperuniform disordered reflectors has been implemented using the Polyjet technique.⁷⁹ Such a waveguide was designed to have a circular hollow core (5 mm in diameter) surrounded by disordered reflector structures that are constructed by dielectric cylinders (113 μm in radius) whose centers follow a distribution of the 3D hyperuniform point pattern [Fig. 6(i)]. The theoretical band diagram presented in Fig. 6(j) shows that the proposed optimal waveguide features a bandgap width of $\sim 21\%$ centered at ~ 410 GHz. Although due to manufacturing precision, the fabricated waveguide was experimentally characterized as having a sub-optimal bandgap of $\sim 15.3\%$ at

290 GHz [Fig. 6(k)], this is still at the largest bandwidth level reported in the literature.^{18,121,123–127} The easily accessible mode field and low propagation loss well below the material bulk absorption loss make such a type of waveguide suitable for sensing applications.

In conclusion, for the above Bragg waveguide-based sensors implemented by 3D printing techniques, the performance and dimensions are limited by the availability of low-loss materials and 3D printing resolutions. Nevertheless, the arbitrary shaping ability of 3D printing techniques greatly simplifies the fabrication process as fabrication of such waveguides using traditional methods is very labor-intensive, and can be said to be almost impossible to achieve waveguides like the hyperuniform disordered waveguide. Therefore,

the further evolution of 3D printing techniques will undoubtedly provide more possibilities for THz waveguide fabrication as well as boost their applications in various fields.

So far, most of the fibers/waveguides that have been demonstrated in the field of THz communications are etched silicon-based waveguides, plastic-drawn-based fibers, and 3D-printed-based thermoplastic/photopolymer waveguides/fibers. At the same time, silicon waveguide technology is only practical for interconnects with lengths up to a few centimeters or for integrated circuits with small footprints. In situations where meter-scale links are needed, such as interconnecting offices in a multi-storey building, communication between stand-alone devices in complex research laboratories or inside of vehicles, and connecting devices in harsh environments like the machines of war or high-security compartmentalized structures, plastic-drawn fibers offer a more viable solution. However, the relatively large dimension of THz fibers (millimeters to centimeters) is problematic for the fiber drawing

technique, which makes it quite difficult for fabricating THz fibers with complex transverse geometries. In this scenario, as the most cost-effective 3D printing technique, the FDM technique is undoubtedly a promising route for realizing meter-scale communication fibers as its resolution can meet most demands within relatively low THz bands, and a variety of low-loss materials are compatible. Therefore, in recent years, the demonstration of FDM printed fibers for medium/long THz communication applications has been proposed. A comprehensive study on THz communication links was presented using FDM printed/extruded rod-in-air fibers,⁸⁸ in which three fibers with different diameters were employed to identify power/loss-limited and dispersion-limited communication modalities. As shown in Figs. 7(a)–7(c), the large-diameter fiber (1.75 mm) has been shown to have a larger loss due to more mode fields confined in the material core, yet also has stronger bending resistance properties. In contrast, relatively small-diameter fibers have less loss but are more susceptible to bending.

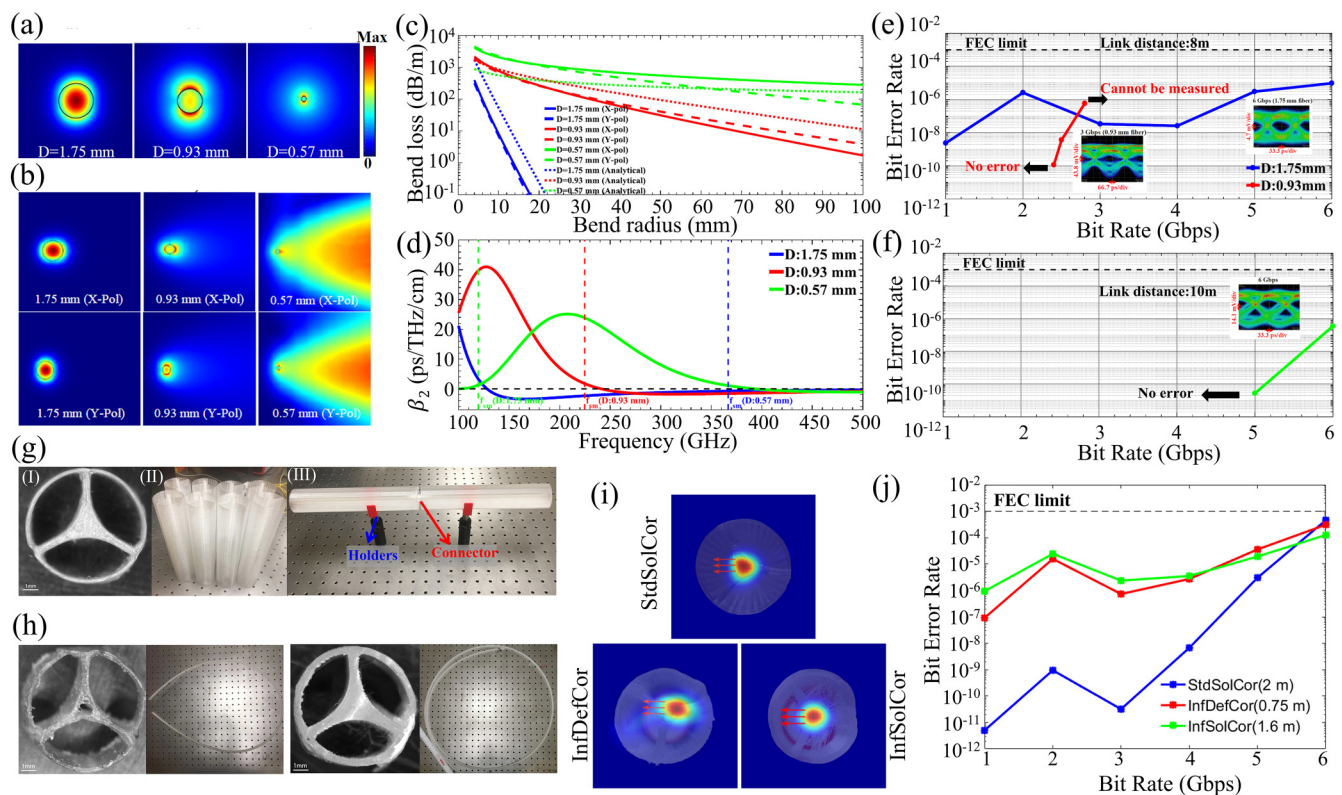


FIG. 7. (a) Normalized electric field distributions of the fundamental mode for the rod-in-air fibers with different diameters (1.75, 0.93, and 0.57 mm) at 128 GHz. (b) The field distributions correspond to those of the bent leaky modes for fibers of different diameters and bending radius of 3 cm. (c) Bending losses of 1.75, 0.93, and 0.57 mm fibers for different bending radii and polarizations. (d) Second-order dispersion of the fundamental mode for 1.75, 0.93, and 0.57 mm fibers. (e) Measured BER vs bit rate for 1.75 and 0.93 mm fibers at a link length of 8 m and the corresponding eye patterns. (f) Measured BER vs bit rate for the 0.57 mm fiber at the link length of 10 m and the eye diagram at 6 Gbps.⁸⁸ Reproduced with permission from Nallappan *et al.*, *Photon. Res.* **8**, 1757–1775 (2020). Copyright 2020 Chinese Laser Press. (g) 3D printed fiber. (h) Cross section, (II) eight of 25 cm-long fiber sections, and (III) two fiber sections connected using one connector and two holders. (i) Two several-meter-long infinity 3D printed fibers: The cross section and side view of the 1.4 m-long (left) and 2.5 m-long fibers (right). (j) Experimentally measured electric field distributions of X-polarized and X-like modes of the three fibers at 128 GHz. Electric field directions are shown as red arrows. (j) Measured BER vs bit rate for three fibers at the carrier frequency of 128 GHz.⁵⁹ From Xu *et al.*, *Sci. Rep.* **12**, 1–13 (2022). Copyright 2022 Author(s), licensed under the Creative Commons Attribution 4.0 International License.

23 August 2023 15:30:10

In addition, fibers of different diameters have very different dispersion characteristics [see Fig. 7(d)]. Therefore, even a communication link (0.93 mm fiber) with a small loss may have a maximum communication rate limited by high link dispersion [see red curve in Fig. 7(e)], whereas a communication link (1.75 mm fiber) with almost zero dispersion at the operating frequency (128 GHz) could be limited by received power [see blue curve in Fig. 7(e)]. Therefore, comprehensive optimization of loss and dispersion is vital to obtain a high-bitrate communication link (0.57 mm fiber) [Fig. 7(f)].

Nevertheless, when using the above-mentioned sub-wavelength air-cladded fibers in practical applications, one should be cautious about adopting advanced encapsulation strategies to protect the air-exposed mode field from perturbations. One feasible solution is to immerse the mode field in a low-loss material (e.g., foam)⁸⁸ or suspend the field within a protective cladding shell¹³³ to resist outer disturbances. However, the poor flexibility of foam-cladded fibers limits the application of such fibers in establishing medium/long communication links; in contrast, suspended core fibers appear to be more practical. Most recently, several meter-scale communication links have been demonstrated using suspended core fibers that were directly fabricated with FDM 3D printing technique.⁵⁸ An advanced optimization process was employed to grant the suspended core fibers with low-loss and near-zero dispersion properties at the operation frequency (128 GHz). The optimized fiber design features a negative curvature core (~1.6 mm) suspended in the center of a protective cladding shell (8 mm in diameter) by three thin bridges (0.4 mm in width). The proposed fiber was first fabricated using traditional/standard FDM 3D printing technique that adopts a vertical extruder, and a 2-m-long communication link was established by mechanically splicing eight individually printed 0.25 m-long fiber sections [Fig. 7(g)]. During the process, well-designed connectors and supporting structures are required to facilitate the successful establishment of the 2-m-long link. The other two fiber links (suspended defect/solid core) [Fig. 7(h)] were implemented by the novel infinity FDM 3D printing technique. Such a technique enables layer-by-layer deposition on a moving conveyor belt through an inclined nozzle, which breaks the volume limitations of traditional FDM printers and allows continuous fabrication of microstructured fibers with the minimal use of supporting structures. The transmission losses of those fabricated fibers were experimentally characterized to be ~3–24 dB/m in the range of 110–150 GHz, which is in the lowest loss range among the reported FDM 3D printed THz fibers.^{82–87} The ability of the fibers to shield the guided mode from external disturbance was also verified with THz imaging of the fiber near-field [Fig. 7(i)]. Furthermore, signal transmission (at 128 GHz) with bit error rate (BER) far below the forward error correction limit (10^{-3}) was demonstrated using three printed fibers at different link lengths [Fig. 7(j)]. This exploration presents for the first time the application of infinity FDM 3D printing technique in the fabrication of THz fibers and successfully established a multi-gigabyte real-time communication link, which reveals that the infinity printed fiber can be an interesting alternative to fiber drawing and extrusion as fiber profiles unlimited in complexity can be fabricated without any process development.

However, although the FDM technique has certain advantages in the fabrication of THz fibers with meter-level lengths and

millimeter-to-centimeter-level structures due to its high production efficiency and cost-effectiveness, its relatively poor resolution is an inherent disadvantage. Therefore, one has to go to high-resolution 3D printing techniques for realizing waveguides/fibers with finer structures (micron scale) or highly integrative functional devices with smaller footprints. But for other high-resolution 3D printing techniques (e.g., SLA, DLP, etc.), high absorption losses of photo-sensitive resins limit their application in the fabrication of direct light-guiding structures (fiber core). Some interesting demonstrations were achieved using 3D-printed guided-optics substrates on which metal layers will be subsequently deposited, thus enabling the propagation of the THz wave through the lossless air between those metal layers.^{65–67} Figure 8(a) presents a dispersion compensator that was printed with the SLA technique and then metalized using wet chemistry deposition technique.⁶⁶ The dispersion compensation functionality was realized by utilizing the anti-crossing of two supermodes (the HE_{11} -like and higher-order modes), which is manifested by the strong curvature in the modal dispersion relation [Fig. 8(b)]. Thus, by operating at the frequency approaching the edges of the bandgap of HE_{11} -like mode [beige regions in Fig. 8(c)], one can achieve very high dispersion in the order of $\sim 10^3$ that can be used as a post-dispersion compensator.

Another interesting example was implementing THz add-drop multiplexers based on metalized SLA-printed two-wire waveguides. The two-wire waveguides have the advantages of almost negligible group velocity dispersion over a broad bandwidth, which makes them suitable for high-speed THz communication applications. Traditionally, two-wire waveguides were implemented by fixing straight wires in bulky holders or by embedding wires into porous dielectric claddings or foams,^{134–136} which is quite labor-intensive and also difficult to precisely maintain the consistency of the gap between two wires. Recently, by metalizing the SLA-printed dielectric two-wire substrate using wet chemistry deposition techniques, a highly reconfigurable encapsulated two-wire waveguide as well as a Y-splitter and a three-ports multiplexer were realized.⁶⁵ The low dispersion characteristic (< 2 ps/THz/cm) of the two-wire waveguide over a broad bandwidth (~ 30 GHz) and the power-splitter/frequency-division functionality of the splitter/multiplexer have been experimentally verified. Based on the above preliminary exploration, a complete four-ports frequency-division multiplexer composed of splitters, couplers, and waveguide Bragg gratings (WBG) was subsequently proposed.⁶⁷ As shown in Figs. 8(d) and 8(e), by optimizing the periods and geometrical parameters of the truncated conical WBG, a high reflection stopband (~ 18 GHz) centered at ~ 140 GHz can be achieved regardless of the nonsymmetric structure of gratings. Figure 8(f) presents a directional coupler implemented using two touched two-wire waveguides (without gratings), the sinusoidal behavior of the coupling coefficients was experimentally demonstrated to be dependent on the length of the coupler [Fig. 8(g)]. Thus, by inscribing Bragg gratings on a pair of joint wires of the coupler, a complete four-ports add-drop multiplexer (ADM) was proposed [Fig. 8(h)]. By optimizing the relative position [L_d^m in Fig. 8(h)] of WBG on the coupler, the proposed ADM can behave under “Optimized Drop Action” (highest output power under the drop action) and Balanced Add/Drop Action (balanced power between the drop and add actions). The communication demonstrations of the developed

23 August 2023 15:30:10

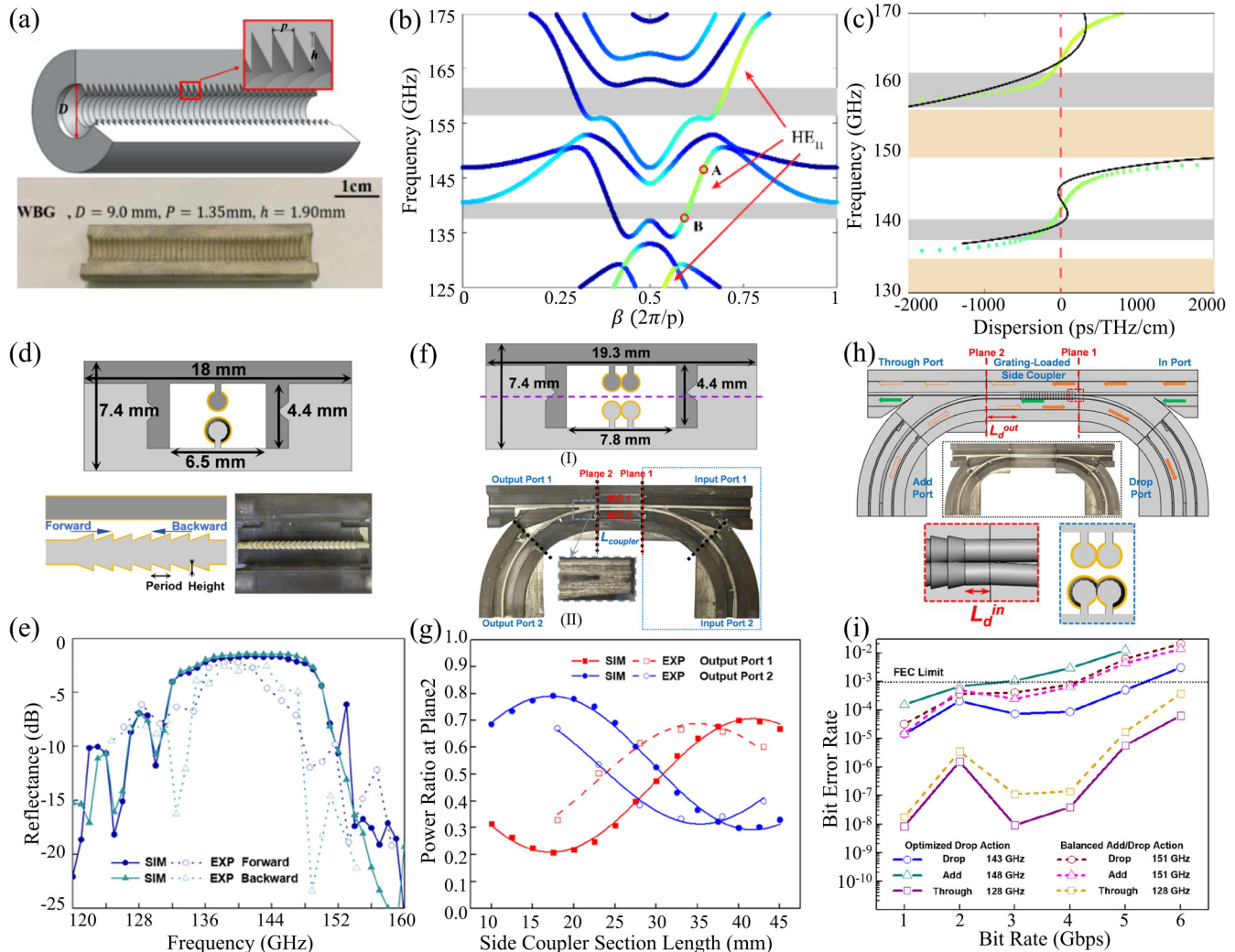


FIG. 8. (a) 3D schematic of the waveguide Bragg grating and a photo of the dissected waveguide Bragg grating. (b) Dispersion relations of the guided modes of the WBG. (c) Comparison between the experimentally measured dispersion (black solid lines) and the theoretically computed dispersion (colored dots) of the fundamental HE_{11} -like mode. Gray regions correspond to the spectral ranges where WBG is effectively single mode. Beige regions refer to the bandgaps of the fundamental HE_{11} -like mode.⁶⁶ Reproduced with permission from Ma *et al.*, Opt. Express **25**, 11009–11026 (2017). Copyright 2017 Optical Society of America. (d) Schematic of the cross section of a two-wire WBG comprising two 3D-printed parts (different shades of gray), its side view and the photograph of a fabricated WBG (top half removed). The gratings featuring a cylindrical sequence of truncated cones (light gray) are suspended in air (white) on dielectric supports and encapsulated within a plastic cage (light and dark gray). Both the cylindrical wire (dark gray) and the gratings are covered with a silver layer (gold) by wet chemistry deposition. (e) The numerical and experimental reflectance (by power) of 2.5 cm-long WBG sections containing 20 periods (Period = 1.03 mm, Height = 0.21 mm). (f) (I) Schematic of the cross section of a straight side coupler. (II) A photo of the assembled directional coupler circuit (top half removed) comprising a side coupler section placed between two Y splitters. The black dashed lines define interfaces between distinct modular sections of the circuit. Inset: the enlarged view of the Y splitter end where curved and straight waveguides meet. (g) The power transmission ratio for output ports 1 and 2 at plane 2 as a function of the side coupler section length. (h) Schematic of the proposed four-port ADM circuit (top part removed) comprising a grating-loaded side coupler placed between two Y splitters. L_d^{in} and L_d^{out} are the distances between the grating end-facets and the side coupler edges (see an inset in the red dotted box). The inset in blue dotted box presents a cross section of the grating-loaded side coupler. Inset in the black dotted box presents an experimental four-port ADM circuit (top part is not shown). (i) Measured BER vs bit rate of the THz carrier wave propagating through two optimized ADM circuits.⁶⁷ From Cao *et al.*, Nat. Commun. **13**, 1–12 (2022). Copyright 2022 Author(s), licensed under the Creative Commons Attribution 4.0 International License.

ADMs with different modalities were carried out and are presented in Fig. 8(i), from which nonsymmetric (symmetric) communication performances for add and drop actions of the ADM with optimized drop (balanced drop/add) action can be clearly observed.

To sum up, 3D printing combined with metallization techniques has been proven feasible for realizing THz waveguides/devices with complex structures and small footprints (~millimeter to centimeter) owing to the high resolution and arbitrary shaping

ability of 3D printing. However, there still remain many challenges, first of all, a great deal of effort is required to obtain good metal layers, especially at complex structural junctions or deep inner surfaces. In addition, some structures (such as junctions, conical structures, etc.⁶⁷) that are difficult to finely print by 3D printing require delicate optimization of the printing process/parameters to facilitate successful printing. Alternatively, such difficult-to-print structures have to be avoided by optimizing the model.⁷¹ Besides, the high absorption loss of photosensitive resins could bring additional loss to the printed waveguide even if the printed substrate is not directly responsible for the transmission of light. So low-loss photosensitive materials are expected to further reduce the loss of such types of waveguides/devices. Furthermore, the build volume of SLA/DLP printers is usually small, which limits the maximum dimensions of the model in a single print, which would introduce additional coupling losses due to the mechanical connection of the individually printed parts. Therefore, cost-effective large-volume SLA/DLP printers are expected to break this limitation.

V. CONCLUSIONS

This paper provides an overview of 3D printing (additive manufacturing) techniques and highlights some recent applications in fabricating THz-guided optics. Specifically, we focus on four commonly used additive manufacturing techniques and their application to THz guided-optics fabrication: vat photopolymerization (SLA/DLP), material jetting (Polyjet), powder bed fusion (SLM), and material extrusion (FDM). We provide detailed examples of 3D-printed THz waveguides, fibers, and functional devices fabricated using these techniques.

The conventional method for fabricating fibers is the fiber drawing technique, which is highly efficient in producing small-diameter fibers (less than a few millimeters). However, this method becomes challenging when attempting to draw larger fibers while maintaining a consistent transverse structure. Moreover, large-diameter drawn fibers (several mm-cm) often exhibit high diameter variation over their length, which limits their practical applications. Consequently, THz microstructured fibers fabricated using the drawing technique are typically short (sub-meter). When the fiber transverse structure is relatively simple, the extrusion technique is generally more suitable for fabricating large-diameter fibers.

Etching on silicon wafers is another popular trend in THz waveguide fabrication, thanks to the process's high manufacturing precision and the high refractive index of the silicon material. However, the etching process is typically confined to a 2D plane, which limits the complexity of waveguide structures that can be produced. Moreover, the microfabrication infrastructure required to produce such devices can be very expensive. Nevertheless, silicon waveguides and devices are excellent candidates for highly integrated THz circuits or on-chip interconnects due to their small footprint and high reliability.

The additive manufacturing technique of 3D printing has several inherent advantages, including the ability to fabricate free-form structures, compatibility with a wide range of materials (such as metal, plastic, ceramics, and more), high manufacturing precision, cost-effectiveness (with less material waste), and high efficiency in fabricating complex structures. As a result, 3D printing

techniques can be used to fabricate various types of THz waveguides, fibers, and devices with complex geometries (such as hyper-uniform disordered waveguides), which are often difficult or even impossible to produce using traditional subtractive fabrication processes. With further development of the 3D printing technique, it is expected that more advanced THz waveguides, fibers, and functional devices can be fabricated, bringing various theoretical concepts closer to reality.

It is worth mentioning that different 3D printing techniques have their own advantages and limitations when it comes to fabricating THz optics. For instance, techniques such as SLA/DLP/Polyjet using photosensitive resin are ideal for creating small optical devices with intricate structures due to their high resolution. However, the resin's high absorption loss (usually greater than 10 cm^{-1}) makes it challenging to produce light-guiding structures that are extended in size, unless high-power sources are available.

To extend the range of applications of high-loss resins, low-loss materials (e.g., air) can be added to the design space, and structural solutions can be used to force a large fraction of light to propagate in low-loss media. Additionally, the high surface smoothness of prints enabled by SLA/DLP/Polyjet techniques makes them suitable for the fabrication of metallic or plasmonic waveguides with the aid of various metallization techniques. Thus, in addition to developing photosensitive resins with lower absorption loss, future research could focus on perfecting augmentation techniques (e.g., thin film metallization), pursuing new ideas and technologies like RECILS, and exploring alternative guiding mechanisms such as plasmonic, ARROW, or photonic-bandgap enabled by high surface quality prints.

At lower THz frequencies ($\sim 0.1\text{ THz}$), standard SLM systems with a resolution above $25\text{ }\mu\text{m}$ offer competitive solutions for the fabrication of reflective freeform THz optics and plasmonic devices compared to standard subtractive techniques, while providing comparable performance. However, at higher frequencies ($\sim 1\text{ THz}$), additional efforts are necessary to improve the surface quality of the devices either through higher-resolution hardware or post-processing. Currently, SLA systems that offer high resolutions (below $25\text{ }\mu\text{m}$) also have a high cost (usually above $\sim 100\text{ K \$}$), which limits their practical applications.

In contrast, the FDM technique is preferable to the aforementioned 3D printing techniques for applications requiring larger or longer devices, especially with the advent of the infinity printing technique, as a wide range of thermoplastics with low absorption loss in the THz range are compatible with the FDM technique. However, the FDM technique has one limitation: its relatively low resolution (usually above $200\text{ }\mu\text{m}$) leads to poor surface finish, which restricts its use to lower THz frequencies ($\sim 0.1\text{ THz}$). Improvements to the FDM technique could involve the development of new materials with optimized rheology and reduced extruded filament diameter. A common limitation of both the SLA and FDM techniques is that the refractive indices of most resins and polymers are limited to the range of $\sim 1.4\text{--}2.0$, resulting in devices with relatively low-to-moderate refractive index contrast. This limitation fundamentally restricts the compactness of integrated or free-space optical devices. Therefore, developing novel 3D printable materials with lower losses and higher refractive indices is an important research direction.

23 August 2023 15:30:10

Currently, 3D printing techniques are mostly used for fabricating THz waveguides and fibers with frequencies well below ~ 1 THz. However, as the frequency increases, the manufacturing precision required also increases. This precision is not only dependent on the printing resolution but also influenced by slicing software and printing settings such as parameters, orientation, and others. Furthermore, advancements in print volumes are required to surpass the limitations of device dimensions that can be produced in a single print. Achieving this may depend more on the emergence of new technologies and innovations in modeling techniques, rather than merely increasing the printer's size. The infinity belt printer is an example of a promising technology that offers a fresh approach to expand the printer's build volume. Ultimately, constant improvements in the performance of 3D printers, along with the decreasing hardware costs, could make these techniques accessible to researchers and laboratories worldwide for THz device fabrication.

ACKNOWLEDGMENTS

M.S. was supported by Canada Research Chairs Tier I in Ubiquitous THz Photonics.

AUTHOR DECLARATIONS

Conflict of Interest

The authors have no conflicts to disclose.

Author Contributions

Guofu Xu: Writing – original draft (equal); Writing – review & editing (equal). **Maksim Skorobogatiy:** Writing – original draft (equal); Writing – review & editing (equal).

DATA AVAILABILITY

Data sharing is not applicable to this article as no new data were created or analyzed in this study.

REFERENCES

- ¹M.-O. Mattsson and M. Simkó, "Emerging medical applications based on non-ionizing electromagnetic fields from 0 Hz to 10 THz," *Med. Devices: Evidence Res.* **12**, 347–368 (2019).
- ²M. J. Fitch and R. Osiander, "Terahertz waves for communications and sensing," *Johns Hopkins APL Tech. Dig.* **25**(4), 348–355 (2004).
- ³D. M. Slocum, E. J. Slingerland, R. H. Giles, and T. M. Goyette, "Atmospheric absorption of terahertz radiation and water vapor continuum effects," *J. Quant. Spectrosc. Radiat. Transfer* **127**, 49–63 (2013).
- ⁴J. Federici and L. Moeller, "Review of terahertz and subterahertz wireless communications," *J. Appl. Phys.* **107**, 111101 (2010).
- ⁵O. P. Cherkasova, D. S. Serdyukov, E. F. Nemova, A. S. Ratushnyak, A. S. Kucheryavenko, I. N. Dolganova, G. Xu, M. Skorobogatiy, I. V. Reshetov, and P. S. Timashev, "Cellular effects of terahertz waves," *J. Biomed. Opt.* **26**, 090902 (2021).
- ⁶T. S. Rappaport, Y. Xing, O. Kanhere, S. Ju, A. Madanayake, S. Mandal, A. Alkhateeb, and G. C. Trichopoulos, "Wireless communications and applications above 100 GHz: Opportunities and challenges for 6G and beyond," *IEEE Access* **7**, 78729–78757 (2019).
- ⁷T. S. Rappaport, S. Sun, R. Mayzus, H. Zhao, Y. Azar, K. Wang, G. N. Wong, J. K. Schulz, M. Samimi, and F. Gutierrez, "Millimeter wave mobile communications for 5G cellular: It will work!," *IEEE Access* **1**, 335–349 (2013).
- ⁸S. Ergün and S. Sönmez, "Terahertz technology for military applications," *J. Manag. Inf. Sci.* **3**, 13–16 (2015).
- ⁹K. Nallappan and M. Skorobogatiy, "Photonics based frequency hopping spread spectrum system for secure terahertz communications," *Opt. Express* **30**, 27028 (2022).
- ¹⁰R. Piesiewicz, M. Jacob, M. Koch, J. Schoebel, and T. Kurner, "Performance analysis of future multigigabit wireless communication systems at THz frequencies with highly directive antennas in realistic indoor environments," *IEEE J. Sel. Top. Quantum Electron.* **14**, 421–430 (2008).
- ¹¹A. Mazhorova, A. Markov, A. Ng, R. Chinnappan, O. Skorobogata, M. Zourob, and M. Skorobogatiy, "Label-free bacteria detection using evanescent mode of a suspended core terahertz fiber," *Opt. Express* **20**, 5344–5355 (2012).
- ¹²B. You, J.-Y. Lu, C.-P. Yu, T.-A. Liu, and J.-L. Peng, "Terahertz refractive index sensors using dielectric pipe waveguides," *Opt. Express* **20**, 5858–5866 (2012).
- ¹³H. Chen, W.-J. Lee, H.-Y. Huang, C.-M. Chiu, Y.-F. Tsai, T.-F. Tseng, J.-T. Lu, W.-L. Lai, and C.-K. Sun, "Performance of THz fiber-scanning near-field microscopy to diagnose breast tumors," *Opt. Express* **19**, 19523–19531 (2011).
- ¹⁴A. Tuniz, K. J. Kaltenecker, B. M. Fischer, M. Walther, S. C. Fleming, A. Argyros, and B. T. Kuhlmeier, "Metamaterial fibres for subdiffraction imaging and focusing at terahertz frequencies over optically long distances," *Nat. Commun.* **4**, 2706 (2013).
- ¹⁵G. Katyba, N. Chernomyrdin, I. Dolganova, A. Pronin, I. Minin, O. Minin, K. Zaytsev, and V. Kurlov, "Step-index sapphire fiber and its application in a terahertz near-field microscopy," in *Millimetre Wave and Terahertz Sensors and Technology XII* (SPIE, 2019), pp. 125–131.
- ¹⁶G. Xu and M. Skorobogatiy, "Wired THz communications," *J. Infrared, Millimeter, Terahertz Waves* **43**, 728–778 (2022).
- ¹⁷K. Nielsen, H. K. Rasmussen, A. J. Adam, P. C. Planken, O. Bang, and P. U. Jepsen, "Bendable, low-loss topas fibers for the terahertz frequency range," *Opt. Express* **17**, 8592–8601 (2009).
- ¹⁸C. S. Ponseca, Jr., R. Pobre, E. Estacio, N. Sarukura, A. Argyros, M. C. Large, and M. A. van Eijkelenborg, "Transmission of terahertz radiation using a microstructured polymer optical fiber," *Opt. Lett.* **33**, 902–904 (2008).
- ¹⁹N. Aflakian, N. Yang, T. LaFave, R. M. Henderson, K. K. O, and D. L. MacFarlane, "Square dielectric THz waveguides," *Opt. Express* **24**, 14951–14959 (2016).
- ²⁰T. Ma, A. Markov, L. Wang, and M. Skorobogatiy, "Graded index porous optical fibers - dispersion management in terahertz range," *Opt. Express* **23**, 7856–7869 (2015).
- ²¹M. Roze, B. Ung, A. Mazhorova, M. Walther, and M. Skorobogatiy, "Suspended core subwavelength fibers: Towards practical designs for low-loss terahertz guidance," *Opt. Express* **19**, 9127–9138 (2011).
- ²²H. Bao, K. Nielsen, H. K. Rasmussen, P. U. Jepsen, and O. Bang, "Fabrication and characterization of porous-core honeycomb bandgap THz fibers," *Opt. Express* **20**, 29507–29517 (2012).
- ²³A. Dupuis, A. Mazhorova, F. Desevedavy, M. Roze, and M. Skorobogatiy, "Spectral characterization of porous dielectric subwavelength THz fibers fabricated using a microstructured molding technique," *Opt. Express* **18**, 13813–13828 (2010).
- ²⁴A. Dupuis, J.-F. Allard, D. Morris, K. Stoeffler, C. Dubois, and M. Skorobogatiy, "Fabrication and THz loss measurements of porous subwavelength fibers using a directional coupler method," *Opt. Express* **17**, 8012–8028 (2009).
- ²⁵A. Argyros, I. M. Bassett, M. A. Van Eijkelenborg, M. C. Large, J. Zagari, N. A. Nicorovici, R. C. McPhedran, and C. M. de Sterke, "Ring structures in microstructured polymer optical fibres," *Opt. Express* **9**, 813–820 (2001).
- ²⁶A. Argyros, S. G. Leon-Saval, and M. A. van Eijkelenborg, "Twin-hollow-core optical fibers," *Opt. Commun.* **282**, 1785–1788 (2009).
- ²⁷L. Wang, Y. Zhang, L. Ren, X. Wang, T. Li, B. Hu, Y. Li, W. Zhao, and X. Chen, "A new approach to mass fabrication technology of microstructured polymer optical fiber preform," *Chin. Opt. Lett.* **3**, S94–S95 (2005).

23 August 2023 15:30:10

- ²⁸Y. Zhang, K. Li, L. Wang, L. Ren, W. Zhao, R. Miao, M. C. J. Large, and A. van Eijkelenborg, "Casting preforms for microstructured polymer optical fibre fabrication," *Opt. Express* **14**, 5541–5547 (2006).
- ²⁹W. Talataisong, R. Ismael, S. R. Sandoghchi, T. Rutirawut, G. Topley, M. Beresna, and G. Brambilla, "Novel method for manufacturing optical fiber: Extrusion and drawing of microstructured polymer optical fibers from a 3D printer," *Opt. Express* **26**, 32007–32013 (2018).
- ³⁰S. Atakaramians, S. Afshar, H. Ebendorff-Heidepriem, M. Nagel, B. M. Fischer, D. Abbott, and T. M. Monro, "THz porous fibers: Design, fabrication and experimental characterization," *Opt. Express* **17**, 14053–14062 (2009).
- ³¹W. Talataisong, J. Gorecki, R. Ismael, M. Beresna, D. Schwendemann, V. Apostolopoulos, and G. Brambilla, "Singlemoded THz guidance in bendable TOPAS suspended-core fiber directly drawn from a 3D printer," *Sci. Rep.* **10**, 11045 (2020).
- ³²W. Talataisong, J. Gorecki, L. D. van Putten, R. Ismael, J. Williamson, K. Addinall, D. Schwendemann, M. Beresna, V. Apostolopoulos, and G. Brambilla, "Hollow-core antiresonant terahertz fiber-based TOPAS extruded from a 3D printer using a metal 3D printed nozzle," *Photon. Res.* **9**, 1513 (2021).
- ³³K. Markstedt, A. Mantas, I. Tournier, H. Martínez Ávila, D. Hagg, and P. Gatenholm, "3D bioprinting human chondrocytes with nanocellulose–alginate bioink for cartilage tissue engineering applications," *Biomacromolecules* **16**, 1489–1496 (2015).
- ³⁴M. S. Mannoor, Z. Jiang, T. James, Y. L. Kong, K. A. Malatesta, W. O. Soboyejo, N. Verma, D. H. Gracias, and M. C. McAlpine, "3D printed bionic ears," *Nano Lett.* **13**, 2634–2639 (2013).
- ³⁵Q. Yan, H. Dong, J. Su, J. Han, B. Song, Q. Wei, and Y. Shi, "A review of 3D printing technology for medical applications," *Engineering* **4**, 729–742 (2018).
- ³⁶S. C. Joshi and A. A. Sheikh, "3D printing in aerospace and its long-term sustainability," *Virtual Phys. Prototyping* **10**, 175–185 (2015).
- ³⁷M. S. Karkun and S. Dharmalingam, "3D printing technology in aerospace industry—A review," *Int. J. Aviat. Aeronaut. Aerospace* **9**(2), 4 (2022).
- ³⁸X. Fu, Y. Lin, X.-J. Yue, B. Hur, and X.-Z. Yue, "A review of additive manufacturing (3D printing) in aerospace: Technology, materials, applications, and challenges," in *Mobile Wireless Middleware, Operating Systems and Applications: 10th International Conference on Mobile Wireless Middleware, Operating Systems and Applications (MOBILWARE 2021)* (Springer International Publishing, Cham, Switzerland, 2022), pp. 73–98.
- ³⁹C. Holt, L. Edwards, L. Keyte, F. Moghaddam, and B. Townsend, "Construction 3D printing," in *3D Concrete Printing Technology* (Elsevier, 2019), pp. 349–370.
- ⁴⁰S. El-Sayegh, L. Romdhane, and S. Manjikian, "A critical review of 3D printing in construction: Benefits, challenges, and risks," *Arch. Civ. Mech. Eng.* **20**, 1–25 (2020).
- ⁴¹Y. W. D. Tay, B. Panda, S. C. Paul, N. A. Noor Mohamed, M. J. Tan, and K. F. Leong, "3D printing trends in building and construction industry: A review," *Virtual Phys. Prototyping* **12**, 261–276 (2017).
- ⁴²T. Spahiu, N. Grimmelsmann, A. Ehrmann, E. Piperi, and E. Shehi, "Effect of 3D printing on textile fabric," in *Proceedings of the 1st International Conference on Engineering and Entrepreneurship* (2017), Vol. 1, pp. 1–7.
- ⁴³M. Korger, J. Bergschneider, M. Lutz, B. Mahltig, K. Finsterbusch, and M. Rabe, "Possible applications of 3D printing technology on textile substrates," in *IOP Conference Series: Materials Science and Engineering* (IOP Publishing, 2016), p. 012011.
- ⁴⁴S. Chakraborty and M. C. Biswas, "3D printing technology of polymer-fiber composites in textile and fashion industry: A potential roadmap of concept to consumer," *Compos. Struct.* **248**, 112562 (2020).
- ⁴⁵T. P. Mpofu, C. Mawere, and M. Mukosera, "The impact and application of 3D printing technology," *Int. J. Sci. Res.* **3**(6), 2148–2152 (2014).
- ⁴⁶N. Shahrubudin, T. C. Lee, and R. Ramlan, "An overview on 3D printing technology: Technological, materials, and applications," *Proc. Manuf.* **35**, 1286–1296 (2019).
- ⁴⁷X. Yu, M. Liang, and C. Shemelya, "3D printable multilayer RF integrated system," in *International Telemetering Conference Proceedings* (2015), Vol. 51, pp. 1–6.
- ⁴⁸T. P. Ketter, Y. Vega, N. C. Arnal, J. W. Stratton, E. A. Rojas-Nastrucci, M. F. Córdoba-Erazo, M. M. Abidin, C. W. Perkowski, P. I. Deffenbaugh, and K. H. Church, "A 2.45 GHz phased array antenna unit cell fabricated using 3-D multi-layer direct digital manufacturing," *IEEE Trans. Microw. Theory Tech.* **63**, 4382–4394 (2015).
- ⁴⁹N. Arnal, T. Ketter, Y. Vega, J. Stratton, C. Perkowski, P. Deffenbaugh, K. Church, and T. Weller, "3D multi-layer additive manufacturing of a 2.45 GHz RF front end," in *2015 IEEE MTT-s International Microwave Symposium* (IEEE, 2015), pp. 1–4.
- ⁵⁰M. I. M. Ghazali, E. Gutierrez, J. C. Myers, A. Kaur, B. Wright, and P. Chahal, "Affordable 3D printed microwave antennas," in *2015 IEEE 65th Electronic Components and Technology Conference (ECTC)* (IEEE, 2015), pp. 240–246.
- ⁵¹J. Kimionis, M. Isakov, B. S. Koh, A. Georgiadis, and M. M. Tentzeris, "3D-printed origami packaging with inkjet-printed antennas for RF harvesting sensors," *IEEE Trans. Microw. Theory Tech.* **63**, 4521–4532 (2015).
- ⁵²J. Allen and B.-I. Wu, "Design and fabrication of an RF GRIN lens using 3D printing technology," in *Terahertz, RF, Millimeter, and Submillimeter-Wave Technology and Applications VI* (SPIE, 2013), pp. 164–170.
- ⁵³X. Zhang and F. Liou, "Introduction to additive manufacturing," in *Additive Manufacturing*, edited by J. Pou, A. Riveiro, and J. Paulo Davim (Elsevier, 2021), pp. 1–31.
- ⁵⁴E. Castro-Camus, M. Koch, and A. I. Hernandez-Serrano, "Additive manufacture of photonic components for the terahertz band," *J. Appl. Phys.* **127**, 210901 (2020).
- ⁵⁵C. Körner, "Additive manufacturing of metallic components by selective electron beam melting—A review," *Int. Mater. Rev.* **61**, 361–377 (2016).
- ⁵⁶M. Schmid, A. Amado, and K. Wegener, "Polymer powders for selective laser sintering (SLS)," *AIP Conf. Proc.* **1664**, 160009 (2015).
- ⁵⁷C. Y. Yap, C. K. Chua, Z. L. Dong, Z. H. Liu, D. Q. Zhang, L. E. Loh, and S. L. Sing, "Review of selective laser melting: Materials and applications," *Appl. Phys. Rev.* **2**, 041101 (2015).
- ⁵⁸G. Xu, K. Nallappan, Y. Cao, and M. Skorobogatiy, "Infinity additive manufacturing of continuous microstructured fiber links for THz communications," *Sci. Rep.* **12**, 4551 (2022).
- ⁵⁹A. von Bieren, E. De Rijk, J.-P. Ansermet, and A. Macor, "Monolithic metal-coated plastic components for mm-wave applications," in *2014 39th International Conference on Infrared, Millimeter, and Terahertz Waves (IRMMW-THz)* (IEEE, 2014), pp. 1–2.
- ⁶⁰M. D'Auria, W. J. Otter, J. Hazell, B. T. W. Gillatt, C. Long-Collins, N. M. Ridler, and S. Lucyszyn, "3-D printed metal-pipe rectangular waveguides," *IEEE Trans. Compon. Packag. Manuf. Technol.* **5**, 1339–1349 (2015).
- ⁶¹W. J. Otter, N. M. Ridler, H. Yasukochi, K. Soeda, K. Konishi, J. Yumoto, M. Kuwata-Gonokami, and S. Lucyszyn, "3D printed 1.1 THz waveguides," *Electron. Lett.* **53**, 471–473 (2017).
- ⁶²M. T. A. Khan, H. Li, N. N. M. Duong, A. Blanco-Redondo, and S. Atakaramians, "3D-printed terahertz topological waveguides," *Adv. Mater. Technol.* **6**(7), 2100252 (2021).
- ⁶³A. L. Cruz, M. A. Franco, C. M. Cordeiro, G. S. Rodrigues, J. H. Osório, and L. E. da Silva, "Exploring THz hollow-core fiber designs manufactured by 3D printing," in *2017 SBMO/IEEE MTT-S International Microwave and Optoelectronics Conference (IMOC)* (IEEE, 2017), pp. 1–5.
- ⁶⁴J. Li, K. Nallappan, H. Guerboukha, and M. Skorobogatiy, "3D printed hollow core terahertz Bragg waveguides with defect layers for surface sensing applications," *Opt. Express* **25**, 4126–4144 (2017).
- ⁶⁵Y. Cao, K. Nallappan, H. Guerboukha, G. Xu, and M. Skorobogatiy, "Additive manufacturing of highly reconfigurable plasmonic circuits for terahertz communications," *Optica* **7**(9), 1112–1125 (2020).
- ⁶⁶T. Ma, K. Nallapan, H. Guerboukha, and M. Skorobogatiy, "Analog signal processing in the terahertz communication links using waveguide bragg gratings: Example of dispersion compensation," *Opt. Express* **25**, 11009–11026 (2017).

- ⁶⁷Y. Cao, K. Nallappan, G. Xu, and M. Skorobogatiy, "Add drop multiplexers for terahertz communications using two-wire waveguide-based plasmonic circuits," *Nat. Commun.* **13**, 1–12 (2022).
- ⁶⁸J. Shen, M. W. Aiken, M. Abbasi, D. P. Parekh, X. Zhao, M. D. Dickey, and D. S. Ricketts, "Rapid prototyping of low loss 3D printed waveguides for millimeter-wave applications," in *2017 IEEE MTT-S International Microwave Symposium (IMS)* (IEEE, 2017), pp. 41–44.
- ⁶⁹B. Hong, M. Swithenbank, N. Greenall, R. G. Clarke, N. Chudpooti, P. Akkarakethalin, N. Somjit, J. E. Cunningham, and I. D. Robertson, "Low-loss asymptotically single-mode THz Bragg fiber fabricated by digital light processing rapid prototyping," *IEEE Trans. Terahertz Sci. Technol.* **8**, 90–99 (2018).
- ⁷⁰A. M. Cook, C. D. Joye, and J. P. Calame, "W-band and D-band traveling-wave tube circuits fabricated by 3D printing," *IEEE Access* **7**, 72561–72566 (2019).
- ⁷¹J. Shen and D. S. Ricketts, "Additive manufacturing of complex millimeter-wave waveguides structures using digital light processing," *IEEE Trans. Microw. Theory Tech.* **67**, 883–895 (2019).
- ⁷²Z. Wu, W. R. Ng, M. E. Gehm, and H. Xin, "Terahertz electromagnetic crystal waveguide fabricated by polymer jetting rapid prototyping," *Opt. Express* **19**, 3962–3972 (2011).
- ⁷³Z. Wu, M. Liang, W.-R. Ng, M. Gehm, and H. Xin, "Terahertz horn antenna based on hollow-core electromagnetic crystal (EMXT) structure," *IEEE Trans. Antennas Propag.* **60**, 5557–5563 (2012).
- ⁷⁴J. Yang, J. Zhao, C. Gong, H. Tian, L. Sun, P. Chen, L. Lin, and W. Liu, "3D printed low-loss THz waveguide based on kagome photonic crystal structure," *Opt. Express* **24**, 22454–22460 (2016).
- ⁷⁵N. Yudasari, J. Anthony, and R. Leonhardt, "Terahertz pulse propagation in 3D-printed waveguide with metal wires component," *Opt. Express* **22**, 26042–26054 (2014).
- ⁷⁶D. W. Vogt and R. Leonhardt, "3D-Printed broadband dielectric tube terahertz waveguide with anti-reflection structure," *J. Infrared Millimeter Terahertz Waves* **37**, 1086–1095 (2016).
- ⁷⁷A. Kaur, J. C. Myers, M. I. M. Ghazali, J. Byford, and P. Chahal, "Affordable terahertz components using 3D printing," in *2015 IEEE 65th Electronic Components and Technology Conference (ECTC)* (IEEE, 2015), pp. 2071–2076.
- ⁷⁸S. Pandey, B. Gupta, and A. Nahata, "Terahertz plasmonic waveguides created via 3D printing," *Opt. Express* **21**, 24422–24430 (2013).
- ⁷⁹T. Ma, H. Guerboukha, M. Girard, A. D. Squires, R. A. Lewis, and M. Skorobogatiy, "3D printed hollow-core terahertz optical waveguides with hyper-uniform disordered dielectric reflectors," *Adv. Opt. Mater.* **4**, 2085–2094 (2016).
- ⁸⁰K. V. Caekenbergh, P. Bley, T. Craeghs, M. Pelk, and S. V. Bael, "A W-band waveguide fabricated using selective laser melting," *Microw. Opt. Technol. Lett.* **54**, 2572–2575 (2012).
- ⁸¹D. Headland, W. Withayachumnankul, M. Webb, H. Ebendorff-Heidepriem, A. Luiten, and D. Abbott, "Analysis of 3D-printed metal for rapid-prototyped reflective terahertz optics," *Opt. Express* **24**, 17384–17396 (2016).
- ⁸²A. L. Cruz, A. Argyros, X. Tang, C. M. Cordeiro, and M. Franco, "3D-printed terahertz Bragg fiber," in *2015 40th International Conference on Infrared, Millimeter, and Terahertz Waves (IRMMW-THz)* (IEEE, 2015), pp. 1–2.
- ⁸³A. L. Cruz, V. A. Serrao, C. L. Barbosa, M. A. Franco, C. M. Cordeiro, A. Argyros, and X. Tang, "3D printed hollow core fiber with negative curvature for terahertz applications," *J. Microw. Optoelectron. Electromag. Appl.* **14**, 45–53 (2015).
- ⁸⁴L. D. van Putten, J. Gorecki, E. Numkam Fokoua, V. Apostolopoulos, and F. Poletti, "3D-printed polymer antiresonant waveguides for short-reach terahertz applications," *Appl. Opt.* **57**, 3953–3958 (2018).
- ⁸⁵S. Li, Z. Dai, Z. Wang, P. Qi, Q. Su, X. Gao, C. Gong, and W. Liu, "A 0.1 THz low-loss 3D printed hollow waveguide," *Optik* **176**, 611–616 (2019).
- ⁸⁶J. Sultana, M. S. Islam, C. M. B. Cordeiro, M. S. Habib, A. Dinovits, M. Kaushik, B. W. H. Ng, H. Ebendorff-Heidepriem, and D. Abbott, "Hollow core inhibited coupled antiresonant terahertz fiber: A numerical and experimental study," *IEEE Trans. Terahertz Sci. Technol.* **11**, 245–260 (2021).
- ⁸⁷Y. Cao, K. Nallappan, H. Guerboukha, T. Gervais, and M. Skorobogatiy, "Additive manufacturing of resonant fluidic sensors based on photonic bandgap waveguides for terahertz applications," *Opt. Express* **27**, 27663–27681 (2019).
- ⁸⁸K. Nallappan, Y. Cao, G. Xu, H. Guerboukha, C. Nerguizian, and M. Skorobogatiy, "Dispersion limited versus power limited terahertz transmission links using solid core subwavelength dielectric fibers," *Photon. Res.* **8**, 1757–1775 (2020).
- ⁸⁹S. Yang, X. Sheng, G. Zhao, and S. Li, "Simple birefringent terahertz fiber based on elliptical hollow core," *Opt. Fiber Technol.* **53**, 102064 (2019).
- ⁹⁰S. Yang, X. Sheng, G. Zhao, Y. Wang, and Y. Yu, "Novel pentagram THz hollow core anti-resonant fiber using a 3D printer," *J. Infrared Millimeter Terahertz Waves* **40**, 720–730 (2019).
- ⁹¹S. Yang, X. Sheng, G. Zhao, S. Lou, and J. Guo, "Anti-deformation low loss double pentagon nested terahertz hollow core fiber," *Opt. Fiber Technol.* **56**, 102199 (2020).
- ⁹²H. Yasukochi, "Three-dimensional modeling apparatus, object, and method of manufacturing an object," U.S. patent 10,022,911 (17 July 2018).
- ⁹³K. Konishi, H. Yasukochi, K. Soeda, Y. Takano, H. Niwa, J. Yumoto, and M. Kuwata-Gonokami, "Thick THz metamaterials fabricated by 3D printer for THz high-pass filter application," in *The European Conference on Lasers and Electro-Optics* (Optica Publishing Group, 2017), p. CC_5_4.
- ⁹⁴A. Hofmann, K. Lomakin, M. Sippel, and G. Gold, "Additively manufactured slotted waveguides for THz applications," in *2022 IEEE/MTT-S International Microwave Symposium-IMS 2022* (IEEE, 2022), pp. 695–698.
- ⁹⁵Z. Wu, W.-R. Ng, M. Gehm, and H. Xin, "Hollow-core electromagnetic band gap (EBG) waveguide fabricated by rapid prototyping for low-loss terahertz guiding," in *2010 IEEE MTT-S International Microwave Symposium* (IEEE, 2010), pp. 644–647.
- ⁹⁶L. Lamagna, A. Paiella, S. Masi, L. Bottini, A. Boschetto, and F. Veniali, "Selective laser melting process of Al-based pyramidal horns for the W-band: Fabrication and testing," *J. Infrared Millimeter Terahertz Waves* **42**, 154–172 (2021).
- ⁹⁷B. Zhang, Z. Zhan, Y. Cao, H. Gulan, P. Linner, J. Sun, T. Zwick, and H. Zirath, "Metallic 3-D printed antennas for millimeter- and submillimeter wave applications," *IEEE Trans. Terahertz Sci. Technol.* **6**, 592–600 (2016).
- ⁹⁸S. Freer, R. Martínez, D. Pérez-Quintana, M. Beruete, S. M. Hanham, M. M. Attallah, and M. Navarro-Cia, "Metal 3D printed D-band waveguide to surface wave transition," in *2020 45th International Conference on Infrared, Millimeter, and Terahertz Waves (IRMMW-THz)* (IEEE, 2020), pp. 1–2.
- ⁹⁹B. Zhang and H. Zirath, "3D printed iris bandpass filters for millimetre-wave applications," *Electron. Lett.* **51**, 1791–1793 (2015).
- ¹⁰⁰B. Zhang and H. Zirath, "Metallic 3-D printed rectangular waveguides for millimeter-wave applications," *IEEE Trans. Compon. Packag. Manuf. Technol.* **6**, 796–804 (2016).
- ¹⁰¹A. I. Hernandez-Serrano and E. Castro-Camus, "Quasi-Wollaston-prism for terahertz frequencies fabricated by 3D printing," *J. Infrared Millimeter Terahertz Waves* **38**, 567–573 (2017).
- ¹⁰²S. F. Busch, M. Koch, E. Castro-Camus, F. Beltrán-Mejía, and J. C. Balzer, "3D-printed tunable THz prism," in *2018 43rd International Conference on Infrared, Millimeter, and Terahertz Waves (IRMMW-THz)* (IEEE, 2018), pp. 1–2.
- ¹⁰³J. M. Seifert, G. G. Hernandez-Cardoso, M. Koch, and E. Castro-Camus, "Terahertz beam steering using active diffraction grating fabricated by 3D printing," *Opt. Express* **28**, 21737–21744 (2020).
- ¹⁰⁴D. Jahn, M. Weidenbach, J. Lehr, L. Becker, F. Beltrán-Mejía, S. F. Busch, J. C. Balzer, and M. Koch, "3D printed terahertz focusing grating couplers," *J. Infrared Millimeter Terahertz Waves* **38**, 708–716 (2017).
- ¹⁰⁵X. P. Dong, J. R. Cheng, F. Fan, S. T. Xu, X. H. Wang, and S. J. Chang, "Wideband sub-THz half-wave plate using 3D-printed low-index metagratings with superwavelength lattice," *Opt. Express* **27**, 202–211 (2019).
- ¹⁰⁶X. Dong, J. Cheng, F. Fan, X. Wang, and S. Chang, "Efficient wide-band large-angle refraction and splitting of a terahertz beam by low-index 3D-printed bilayer metagratings," *Phys. Rev. Appl.* **14**(1), 014064 (2020).
- ¹⁰⁷X. Li, Z. Liu, D. Yan, J. Li, J. Li, G. Qiu, X. Hou, and G. Cheng, "Experimental demonstration of 3D printed terahertz polarization-insensitive flat devices based on low-index meta-gratings," *J. Phys. D: Appl. Phys.* **53**(50), 505301 (2020).

23 August 2023 15:30:10

- ¹⁰⁸S. F. Busch, M. Weidenbach, J. C. Balzer, and M. Koch, "THz optics 3D printed with TOPAS," *J. Infrared Millimeter Terahertz Waves* **37**, 303–307 (2015).
- ¹⁰⁹A. D. Squires, E. Constable, and R. A. Lewis, "3D printed terahertz diffraction gratings and lenses," *J. Infrared Millimeter Terahertz Waves* **36**, 72–80 (2015).
- ¹¹⁰J. Colla, R. Vickers, M. Nancarrow, and R. Lewis, "3D printing metallised plastics as terahertz reflectors," *J. Infrared Millimeter Terahertz Waves* **40**, 752–762 (2019).
- ¹¹¹C. D. Fisher, A. C. Paoella, C. Corey, D. Foster, and D. Silva-Saez, "3-D printed millimeter wave quasi-optical lens system for 60 and 100 GHz applications," in *2019 IEEE Radio and Wireless Symposium (RWS)* (IEEE, 2019), pp. 1–3.
- ¹¹²W. D. Furlan, V. Ferrando, J. A. Monsoriu, P. Zagrajek, E. Czerwinska, and M. Szustakowski, "3D printed diffractive terahertz lenses," *Opt. Lett.* **41**, 1748–1751 (2016).
- ¹¹³C. Liu, L. Niu, K. Wang, and J. Liu, "3D-printed diffractive elements induced accelerating terahertz airy beam," *Opt. Express* **24**, 29342–29348 (2016).
- ¹¹⁴K. Szkudlarek, M. Sypek, G. Cywinski, J. Suszek, P. Zagrajek, A. Feduniewicz-Zmuda, I. Yahniuk, S. Yatsunenko, A. Nowakowska-Siwinska, D. Coquillat, D. B. But, M. Rachon, K. Wegrzynska, C. Skierbiszewski, and W. Knap, "Terahertz 3D printed diffractive lens matrices for field-effect transistor detector focal plane arrays," *Opt. Express* **24**, 20119–20131 (2016).
- ¹¹⁵X. Wei, C. Liu, L. Niu, Z. Zhang, K. Wang, Z. Yang, and J. Liu, "Generation of arbitrary order Bessel beams via 3D printed axicons at the terahertz frequency range," *Appl. Opt.* **54**, 10641–10649 (2015).
- ¹¹⁶Q. Chapdelaine, K. Nallappan, Y. Cao, H. Guerboukha, N. Chernomyrdin, K. Zaytsev, and M. Skorobogatiy, "Fabrication and characterization of a composite TiO₂-polypropylene high-refractive-index solid immersion lens for super-resolution THz imaging," *Opt. Mater. Express* **12**, 3015–3031 (2022).
- ¹¹⁷T. Yu, X. Zuo, W. Liu, and C. Gong, "0.1 THz super-resolution imaging based on 3D printed confocal waveguides," *Opt. Commun.* **459**, 124896 (2020).
- ¹¹⁸Y. Zhu, T. Tang, S. Zhao, D. Joralmon, Z. Poit, B. Ahire, S. Keshav, A. R. Raje, J. Blair, and Z. Zhang, "Recent advancements and applications in 3D printing of functional optics," *Addit. Manuf.* **52**, 102682 (2022).
- ¹¹⁹H. Qu, T. Brastaviceanu, F. Bergeron, J. Olesik, I. Pavlov, T. Ishigure, and M. Skorobogatiy, "Photonic bandgap Bragg fiber sensors for bending/displacement detection," *Appl. Opt.* **52**, 6344–6349 (2013).
- ¹²⁰K. Stoeffler, C. Dubois, A. Ajji, N. Guo, F. Boismenu, and M. Skorobogatiy, "Fabrication of all-polymeric photonic bandgap Bragg fibers using rolling of coextruded PS/PMMA multilayer films," *Polym. Eng. Sci.* **50**, 1122–1127 (2010).
- ¹²¹A. Dupuis, K. Stoeffler, B. Ung, C. Dubois, and M. Skorobogatiy, "Transmission measurements of hollow-core THz Bragg fibers," *J. Opt. Soc. Am. B* **28**, 896–907 (2011).
- ¹²²B. Ung, A. Dupuis, K. Stoeffler, C. Dubois, and M. Skorobogatiy, "High-refractive-index composite materials for terahertz waveguides: Trade-off between index contrast and absorption loss," *J. Opt. Soc. Am. B* **28**, 917–921 (2011).
- ¹²³M. Skorobogatiy and A. Dupuis, "Ferroelectric all-polymer hollow bragg fibers for terahertz guidance," *Appl. Phys. Lett.* **90**, 113514 (2007).
- ¹²⁴A. Hassani, A. Dupuis, and M. Skorobogatiy, "Porous polymer fibers for low-loss terahertz guiding," *Opt. Express* **16**, 6340–6351 (2008).
- ¹²⁵R.-J. Yu, B. Zhang, Y.-Q. Zhang, C.-Q. Wu, Z.-G. Tian, and X.-Z. Bai, "Proposal for ultralow loss hollow-core plastic Bragg fiber with cobweb-structured cladding for terahertz waveguiding," *IEEE Photon. Technol. Lett.* **19**, 910–912 (2007).
- ¹²⁶G. Ren, Y. Gong, P. Shum, X. Yu, and J. Hu, "Polarization maintaining air-core bandgap fibers for terahertz wave guiding," *IEEE J. Quantum Electron.* **45**, 506–513 (2009).
- ¹²⁷K. Nielsen, H. K. Rasmussen, P. U. Jepsen, and O. Bang, "Porous-core honeycomb bandgap THz fiber," *Opt. Lett.* **36**, 666–668 (2011).
- ¹²⁸C.-H. Lai, B. You, J.-Y. Lu, T.-A. Liu, J.-L. Peng, C.-K. Sun, and H.-C. Chang, "Modal characteristics of antiresonant reflecting pipe waveguides for terahertz waveguiding," *Opt. Express* **18**, 309–322 (2010).
- ¹²⁹B. You, J.-Y. Lu, J.-H. Liou, C.-P. Yu, H.-Z. Chen, T.-A. Liu, and J.-L. Peng, "Subwavelength film sensing based on terahertz anti-resonant reflecting hollow waveguides," *Opt. Express* **18**, 19353–19360 (2010).
- ¹³⁰B. You and J.-Y. Lu, "Remote and *in situ* sensing products in chemical reaction using a flexible terahertz pipe waveguide," *Opt. Express* **24**, 18013–18023 (2016).
- ¹³¹R. Singh, W. Cao, I. Al-Naib, L. Cong, W. Withayachumnankul, and W. Zhang, "Ultrasensitive terahertz sensing with high-Q Fano resonances in metasurfaces," *Appl. Phys. Lett.* **105**, 171101 (2014).
- ¹³²R. Singh, I. A. Al-Naib, M. Koch, and W. Zhang, "Sharp Fano resonances in THz metamaterials," *Opt. Express* **19**, 6312–6319 (2011).
- ¹³³K. Dens, J. Vaes, S. Ooms, M. Wagner, and P. Reynaert, "A PAM4 dielectric waveguide link in 28 nm CMOS," in *ESSCIRC 2021-IEEE 47th European Solid State Circuits Conference (ESSCIRC)* (IEEE, 2021), pp. 479–482.
- ¹³⁴M. Mbonye, R. Mendis, and D. M. Mittleman, "A terahertz two-wire waveguide with low bending loss," *Appl. Phys. Lett.* **95**, 233506 (2009).
- ¹³⁵A. Markov, H. Guerboukha, and M. Skorobogatiy, "Hybrid metal wire-dielectric terahertz waveguides: Challenges and opportunities," *J. Opt. Soc. Am. B* **31**, 2587 (2014).
- ¹³⁶A. Markov and M. Skorobogatiy, "Two-wire terahertz fibers with porous dielectric support," *Opt. Express* **21**, 12728–12743 (2013).